

**OPTIMIZATION FOR POWER TRANSMISSION SYSTEM OF UPPER
LIMBS REHABILITATION DEVICE**

JOHN CHAN DE-XING

**A project report submitted in partial fulfilment of the
requirements for the award of Master of Engineering
(Mechanical)**

**Lee Kong Chian Faculty of Engineering and Science
Universiti Tunku Abdul Rahman**

October 2016

DECLARATION

I hereby declare that this project report is based on my original work except for citations and quotations which have been duly acknowledged. I also declare that it has not been previously and concurrently submitted for any other degree or award at UTAR or other institutions.

Signature : _____

Name : _____

ID No. : _____

Date : _____

APPROVAL FOR SUBMISSION

I certify that this project report entitled “**OPTIMIZATION FOR POWER TRANSMISSION SYSTEM OF UPPER LIMBS REHABILITATION DEVICE**” was prepared by **JOHN CHAN DE-XING** has met the required standard for submission in partial fulfilment of the requirements for the award of Master of Engineering(Mechanical) at Universiti Tunku Abdul Rahman.

Approved by,

Signature : _____

Supervisor : _____

Date : _____

The copyright of this report belongs to the author under the terms of the copyright Act 1987 as qualified by Intellectual Property Policy of Universiti Tunku Abdul Rahman. Due acknowledgement shall always be made of the use of any material contained in, or derived from, this report.

© 2016, John Chan. All right reserved.

Specially dedicated to
my beloved mother and father

ACKNOWLEDGEMENTS

I would like to thank everyone who had contributed to the successful completion of this project. I would like to express my gratitude to my research supervisor, Mr. Chuah Yea Dat for his invaluable advice, guidance and his enormous patience throughout the development of the research.

In addition, I would also like to express my gratitude to my loving parent and friends who had helped and given me encouragement.

OPTIMIZATION FOR POWER TRANSMISSION SYSTEM OF UPPER LIMBS REHABILITATION DEVICE

ABSTRACT

People who have a medical condition such as a stroke have lost their motor movement. Thus the exoskeletons for upper limbs rehabilitation were built to train the injured limbs of the patients. This report aims to develop a mechanical based exoskeleton device using rack and pinion mechanisms, and linkages to transmit the input torque from the base of the device to its limbs. The chosen mechanical actuators of the proposed exoskeleton to be optimized were its parallelogram linkages. Some exoskeleton designs that were mentioned in literature have actuators that are positioned directly at the joints. However, existing actuators of the exoskeletons in general are heavy, noisy and have a limited output torque (Gopura, et al., 2011). This makes the limbs heavier which could potentially affect the output strength of these exoskeleton devices in general. The methodology used in this study starts by sketching the proposed exoskeleton while its chosen parts were calculated, modelled, undergo stress analysis and structural optimization to produce an optimized version of the parts. These optimized parts are then calculated, modelled and the stress analysis procedure is repeated for these parts. The outcome of this study is the development and optimization of the proposed exoskeleton. The finite element analysis results of the optimized parts presented in this study shows that the stresses and deflections generated does not exceed the maximum allowable yield stress and deflections compared to their un-optimized counterparts. The achievement obtained from this study is the development of an exoskeleton that is capable of transmitting the input torque mechanically from the base to the limbs without the use of cables, pneumatic and hydraulic pistons. There is a possibility that this exoskeleton can be used to improve the current existing exoskeletons in hospitals that have actuators positioned at their joints.

TABLE OF CONTENTS

DECLARATION	ii
APPROVAL FOR SUBMISSION	iii
ACKNOWLEDGEMENTS	vi
ABSTRACT	vii
TABLE OF CONTENTS	viii
LIST OF FIGURES	x

CHAPTER

1	INTRODUCTION	13
	1.1 Aim	15
	1.2 Objectives	15
	1.3 Scope of Project	16
	1.4 Thesis structure	17
2	LITERATURE REVIEW	18
	2.1 Spring Actuation Design	18
	2.2 Pneumatic Actuation Design	19
	2.3 Cable Actuation Design	20
	2.4 Electromagnetic Motor Actuation Design	21
	2.5 Basics and literature of the Finite Element Method	22
	2.6 Human Isometric Strength	24
	2.7 Summary	26
3	METHODOLOGY	28
	3.1 Workflow	28

4	RESULTS AND DISCUSSION	32
4.1	Overview	32
4.2	Working Principle of Exoskeleton	33
4.3	Solidworks settings	37
4.4	Overview of Calculation of the Exoskeleton's Parts	39
4.4.1	Calculation of the Forearm Part	44
4.4.2	Calculation for Part B	52
4.4.3	Calculation for Part D	58
4.4.4	Calculation for Part E	59
4.4.5	Calculation for the Upper Arm part	60
4.5	FEA results for the exoskeleton parts	63
4.6	Modelling of the optimized structures	69
4.7	Overview of Calculation for the Optimized PartB and Forearm	70
4.7.1	Calculation for the Optimized Forearm Part	71
4.7.2	Calculation for the Optimized Part B	73
4.8	Overview Calculation for the Optimized Part D, E and the upperarm	75
4.8.1	Calculation for the Optimized Part D	83
4.8.2	Calculation for the Optimized Part E	86
4.8.3	Calculation for the Optimized Upper arm	90
4.9	FEA results for the optimized exoskeleton parts.	93
4.10	Discussion	101
5	CONCLUSION AND FUTURE WORKS	104
5.1	Conclusion	104
5.2	Future works	105
5	REFERENCES	106

LIST OF FIGURES

FIGURE	TITLE	PAGE
Figure 2.1	Wu, et al., (2011) exoskeleton	18
Figure 2.2	Pneu-Wrex Exoskeleton (Sanchez, et al., 2005).	19
Figure 2.3	Actuation of the L-EXOS joint(Frisoli, et al., 2005)	20
Figure 2.4	Naidu, et al., (2011) modified exoskeleton design	21
Figure 2.5	Derivation of the matrix formula for a Bar element for FEA learnt from Abbey's (2016) training video	22
Figure 2.6	Human Arm Degree of Freedom (Carignan and Liszka, 2005 cited in Naidu, 2011).	25
Figure 3.1	Research Cycle	28
Figure 4.1	Proposed Exoskeleton	33
Figure 4.2	Proposed Exoskeleton Range of Motion 1	34
Figure 4.3	Proposed Exoskeleton Range of Motion 2	35
Figure 4.4	Part A	37
Figure 4.5	Deflection formulas taken from Pytel and Kiusalaas (2012)	43
Figure 4.6	Diagrams for the cross section-x of the Fore Arm Part. Diagram (b) is generated according to theory given by Learn Easy (2013)	44
Figure 4.7	Load, Shear and Moment Diagram for cross section- x of the forearm	46
Figure 4.8	Diagrams for the cross section-Y of the Fore Arm Part	49

Figure 4.9 Diagrams for Part B. Diagram (b) is generated according to theory given by Learn Easy (2013)	53
Figure 4.10 Load, Moment, Shear Diagram for the cross section x-x of Part B	54
Figure 4.11 Upperarm Diagram	60
Figure 4.12 Part D FEA results (a) von mises stress results for Part D (b) deflection results for Part D	64
Figure 4.13 Part E FEA results (a) von mises stress results for Part E (b) deflection results for Part E	65
Figure 4.14 Upper Arm FEA results (a) von mises stress results for the upper arm (b) deflection results for the upper arm	66
Figure 4.15 Part B FEA results (a) von mises stress results for Part B (b) deflection results for Part B	67
Figure 4.16 lowerarm part FEA results (a) von mises stress results for the lower arm (b) deflection results for the lower arm	68
Figure 4.17 Truss Models	69
Figure 4.18 Truss template developed from Lovett's (2013) tutorials and the intuitively calculated tapering plan.	76
Figure 4.19 Ring Bolt Hole Plan	82
Figure 4.20 Optimized Part D FEA results (a) von mises stress results for the optimized Part D (b) deflection results for the optimized Part D	95
Figure 4.21 Optimized Part E FEA results (a) von mises stress results for the optimized Part E (b) deflection results for the optimized Part E	96
Figure 4.22 Optimized Upper Arm FEA results (a) von mises stress results for the optimized upper arm (b) deflection results for the optimized upper arm	97
Figure 4.23 Optimized part B FEA results (a) von mises stress results for the optimized Part B (b) deflection results for the optimized Part B	98

Figure 4.24 Optimized Lower Arm FEA results(a) von mises stress results for the optimized Lower arm (b)

CHAPTER 1

INTRODUCTION

People who have a medical condition such as a stroke suffer the loss of their motor movement and requires medical treatment or a hospital device to help them regain their motor strength. Exoskeletons for rehabilitation purposes are one of such medical devices meant to train the injured limbs of the aforementioned patients. In recent research related to robotics, exoskeleton systems are a highly active research area (Gopura, et al., 2011). However the research and development for the optimization of upper extremity exoskeleton structures in general are lacking to the author's knowledge.

Some exoskeleton designs have actuators that are positioned directly at the joints. However, existing actuators used by exoskeletons in general are heavy, noisy and have a limited output torque (Gopura, et al., 2011). This could mean the exoskeleton's output torque can be affected by the weight of its actuators if they are significantly heavy enough to affect its entire mechanical system.

The method of using cables with the intent to relocate the actuators to the base of the robot has been used (Frisoli, et al., 2005). However, these cables have the tendency to frail at small cracks that are hard to detect and could potentially cause sudden mechanical failure leading to unwanted injury or death.

The use of electromagnetic motors directly at the limbs of an exoskeleton in general could potentially risk the patient being exposed to the life wiring of the motors

and the robot's frame if metal is used to construct its limbs. Such exoskeleton devices must not be exposed to conductive liquids to avoid unwanted accidents.

The use of springs in exoskeleton devices to apply resistive forces to the patient's movements (Wu, et al., 2011) can be hazardous if these springs are positioned near the user. That is these springs could potentially break if they have rusted or are not properly secured. The use of pneumatic pistons in exoskeleton systems (Sanchez, et al., 2005) however has problems related to leakages and they risk the patient to be near pressurised devices in general. The working principals of a pneumatic piston are similar to that of a hydraulic piston in general meaning that these two methods of actuation is intuitively predicted to have the same problems.

Thus a mechanical based exoskeleton device to transmit the power from the base of the device to its limbs without the use of cables, pneumatic or hydraulic actuators is needed to improve the existing exoskeleton designs mentioned in literature. The present paper presents the development of this mechanical based exoskeleton and the optimization of its chosen parts to reduce the material usage of this device. The chosen mechanical actuators of the proposed exoskeleton to be optimized were its parallelogram linkages.

The exoskeleton was sketched and its parts were calculated, modelled and, undergoes the stress analysis and structural optimization processes. The optimized parts were then calculated, modelled and the stress analysis process was repeated for these parts. The simulation results show that the stresses and deflections generated onto the three-dimensional models of the optimized parts does not exceed the maximum allowable yield stress and deflections compared to their un-optimized counterparts.

1.1 Aim

To design a mechanical based exoskeleton device using rack and pinion mechanisms, cams and linkages to transmit the input torque from the base of the device to its limbs.

1.2 Objectives

1. To plan and sketch the exoskeleton device
2. To choose its mechanical actuators, namely its parallelogram linkage to be optimized
3. To produce a 3D model on the selected components of the exoskeleton by use of Solidworks
4. To perform stress analysis on the selected components of the exoskeleton device
5. To perform structural optimization on the selected components of the exoskeleton device to generate an optimized version of these components
6. To produce a 3D model on the optimized components of the exoskeleton by use of Solidworks
7. To perform stress analysis on the optimized components of the exoskeleton device

1.3 Scope of Project

Figure 4.1 shows the proposed exoskeleton where the mechanical actuators to be optimized in this study were the 2 parallelogram linkages of this device.

This report aims to improve the exoskeleton designs that have actuators located at their joints described in literature by implementing a new exoskeleton system that solves the design problem related to the need to place heavy or expensive actuators at the links without the use of pneumatic or hydraulic pistons and cables.

The objectives of this project were to sketch the proposed exoskeleton followed by, modelling of the proposed exoskeleton's chosen structures, to conduct a structural analysis upon these structures, and to structurally optimize these structures according to the results obtained from the previous structural analysis processes. The optimized parts were then modelled and undergo structural analysis.

This exoskeleton device will be using purely mechanical systems such as rack and pinion mechanisms, cams and linkages to transmit the input torque from the base of the exoskeleton to its limbs.

Different types of actuators can be bought from the market to control the inputs of the proposed exoskeleton's system but this task is reserved for future research. There is a possibility that the proposed exoskeleton designed to position heavy actuators to the base of this device could improve the existing exoskeletons in hospitals. Thus the rational of this research was to improve the exoskeleton devices used in hospitals for rehabilitation purposes.

1.4 Thesis structure

Chapter 1 introduces the report and the aims, objectives and, scope of the projects were described. Chapter 2 discuss on the literature review of the study. The literature review discuss on the actuators used in exoskeletons developed by other researchers in this section of the report. The literature review also discuss on the basics of the finite element method and the Human Isometric Strength taken from Naidu's (2011) paper. Chapter 3 discuss the research methodology used in this study. Chapter 4 however discuss the working principals of the exoskeleton, the settings used in solidworks, the calculations done onto the exoskeleton's parts, the FEA results produced from the parts, the modelling images for some the optimized parts, the calculations done onto the optimized parts, the FEA results produced from the optimized parts. Chapter 5 discuss on the discussions made in this report and the conclusion of the report.

CHAPTER 2

LITERATURE REVIEW

2.1 Spring Actuation Design

Figure 2.1 shows an example of an exoskeleton that uses springs for its actuation. Wu, et al., (2011) designed this exoskeleton to provide muscle training to patients or healthy users to improve the user's muscles and health. The springs of the exoskeleton can be relocated to intensify the muscle training of the user (Wu, et al., 2011).

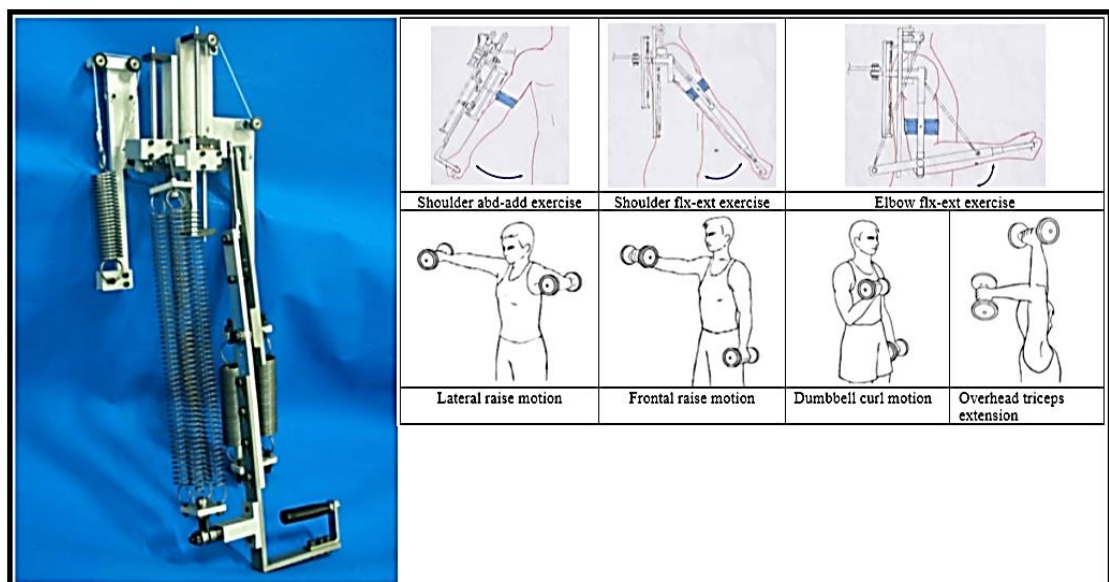


Figure 2.1 Wu, et al., (2011) exoskeleton

2.2 Pneumatic Actuation Design

Figure 2.2 shows an example of an exoskeleton that uses pneumatic actuators for its actuation. The Pneu-Wrex is a robotic version of the passive exoskeleton T-WREX and it uses pneumatic actuators to actuate it (Sanchez, et al., 2005). The T-WREX that is actuated by rubber bands does not restore the full range of motion to the patient's arm as it could only apply a fix pattern of forces onto the user's arm. The T-WREX exoskeleton could vary the magnitude of the gravity balance by manipulating the number of rubber bands used. Such methods however do not provide dynamic patterns of the resistive forces. Current study in robot-assisted movement advices that the dynamic patterns of these resistive forces if used in exoskeletons enhances motor recovery (Sanchez, et al., 2005).

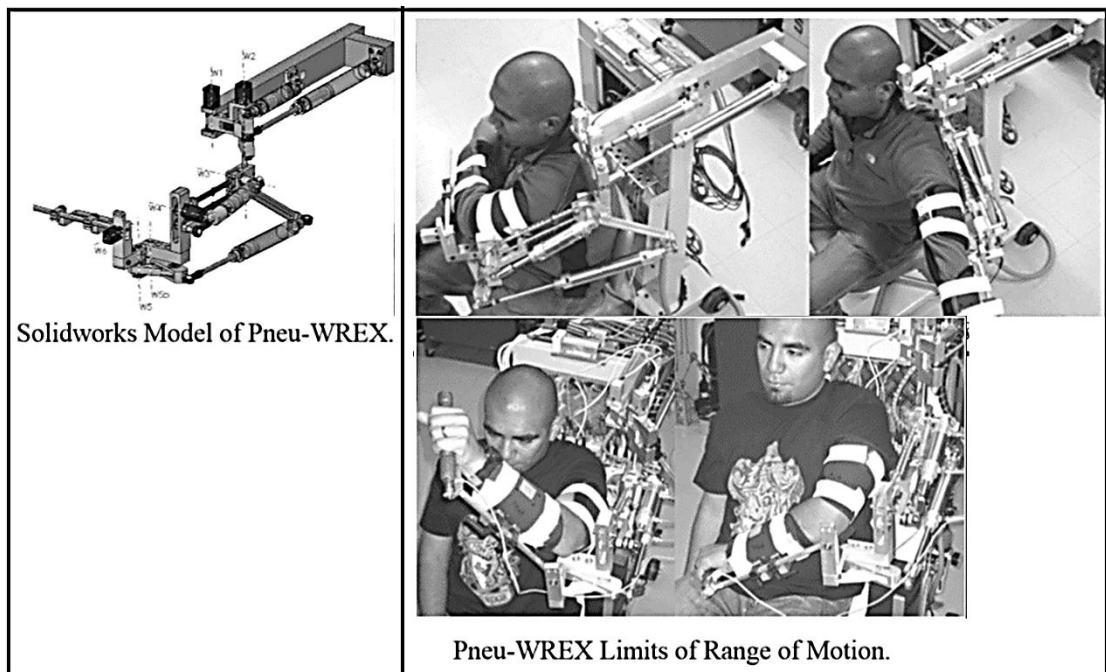


Figure 2.2 Pneu-Wrex Exoskeleton (Sanchez, et al., 2005).

2.3 Cable Actuation Design

Figure 2.3 shows an example of an exoskeleton that uses cables for its actuation. This exoskeleton named as the L-EXOS uses carbon fibre parts and special mechanical components to optimize its design for high stiffness and mass reduction (Frisoli, et al., 2005). All the motors of the exoskeleton are located at the base labelled as Link 0. These motors use steel cables to transmit their torque from link 0 to the reduction gears that are integrated to the joints of this exoskeleton. Figure 2.3 graphically shows this scheme where a motor drives the steel cables that are connected to the reduction gears at axis 2 to control link 2 (Frisoli, et al., 2005).

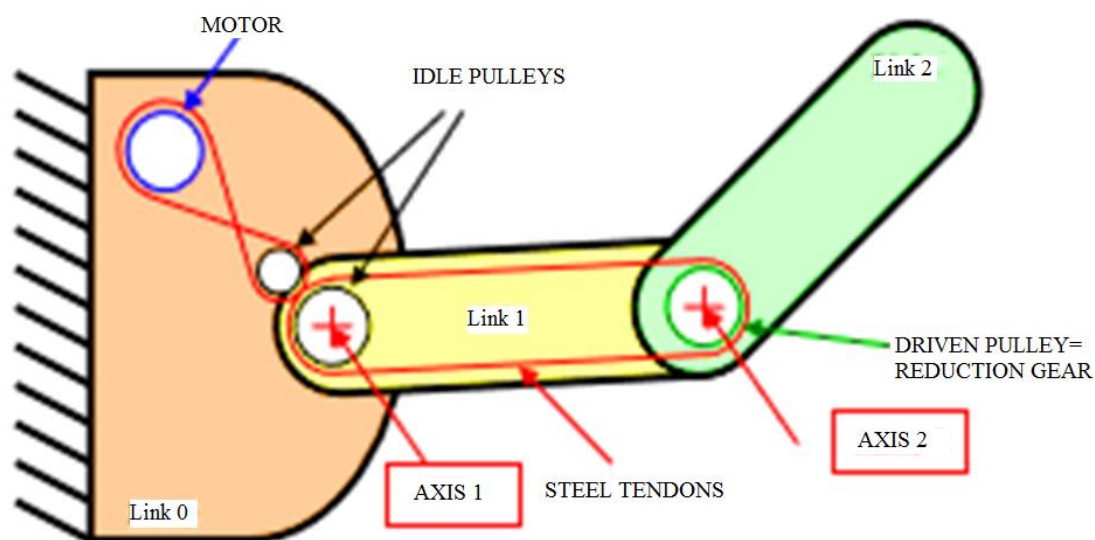
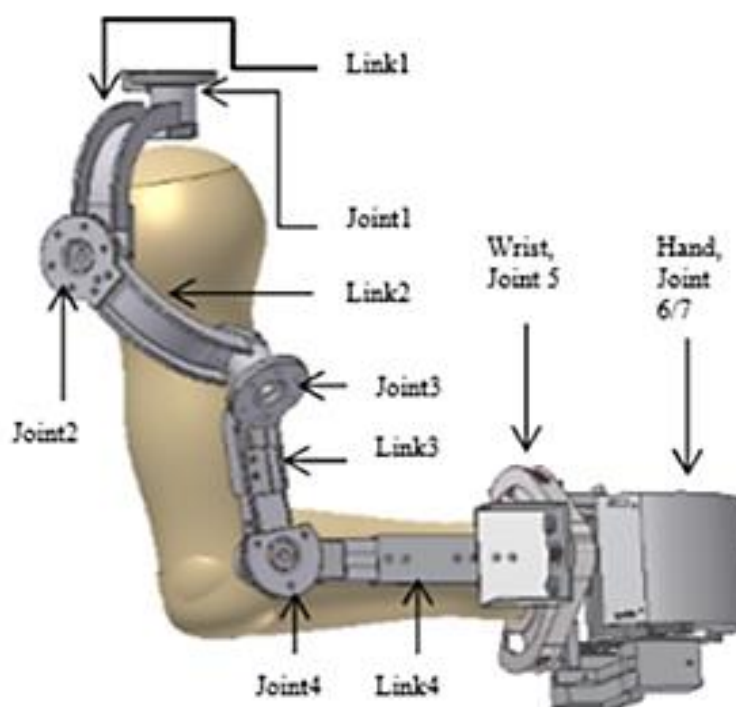


Figure 2.3 Actuation of the L-EXOS joint (Frisoli, et al., 2005)

2.4 Electromagnetic Motor Actuation Design

Figure 2.4 shows an example of an exoskeleton that uses electromagnetic motors for its actuation. This exoskeleton device shown in Figure 2.4 does not need extent support and provides a large workspace with the intent to assist patients who have lost their upper limb motor functions (Naidu, et al., 2011). A previous version of this exoskeleton known as the MGA exoskeleton runs on electric motors located at its joints. Naidu, et al.,'s (2011) proposed design is similar to the MGA but it includes a hand and wrist design (Naidu, et al., 2011).



Final design- complete assembly of shoulder, elbow, wrist and hand designs.

Figure 2.4 Naidu, et al., (2011) modified exoskeleton design

2.5 Basics and literature of the Finite Element Method

According to Abbey's (2016) training video, the general formula used in FEA simulations is known as;

$$[F] = [K][u] \quad (1)$$

Where,

F=force vector, N

K=stiffness matrix, Nm^{-1}

u=displacement vector, m

Figure 2.5 shows the derivation of the matrix formula for a bar element used in FEA simulations. From Abbey's (2016) training video it can be intuitively learnt that the matrix formula derived in Figure 2.5 is used to calculate the displacements 'u' of a group of elements that are arranged to form a 3D mesh structure (Abbey, 2016).

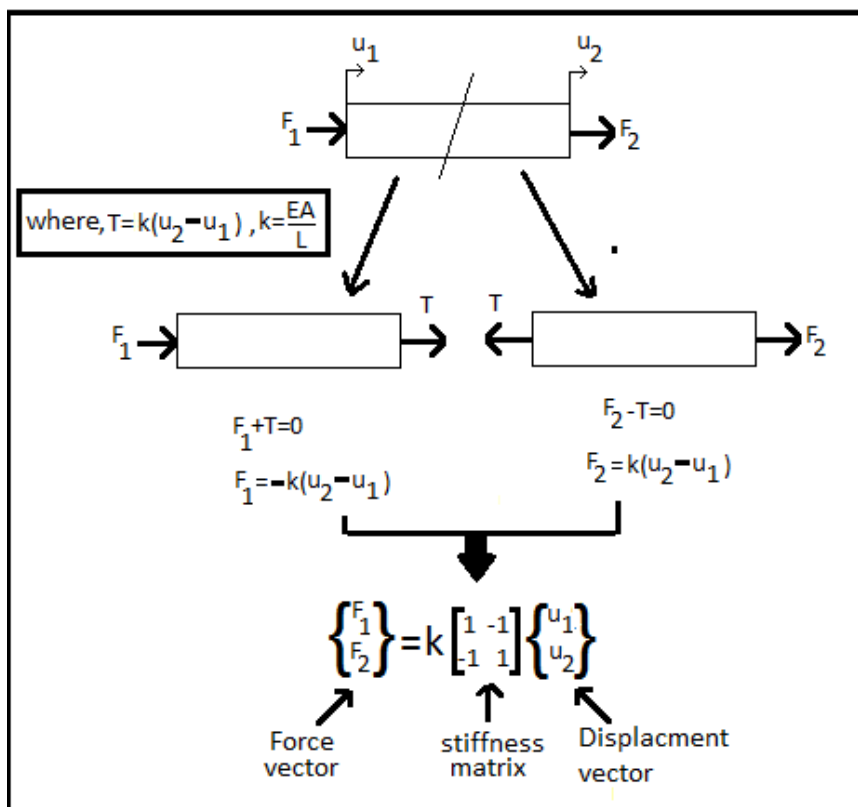


Figure 2.5 Derivation of the matrix formula for a Bar element for FEA learnt from Abbey's (2016) training video

Where,

A =Area

E = *Young Modulus of the bar element, Pa*

u_1 =displacement, m

u_2 =displacement, m

F_1 =Force, N

F_2 =Force, N

T =Tensional Force, N

L =Length of the bar element, m

The displacements of these elements obtained from the displacement vector in Figure 2.5 can be used to calculate their respective strain using;

$$\varepsilon = \frac{u}{L} \quad (\text{Abbey, 2016}) \quad (2)$$

Where

ε = *strain*

u = *displacement vector from Figure 2.5,m*

L = *length of the bar element,m*

The strains obtained from equation (2) can be used to calculate their respective stresses using;

$$\sigma = E\varepsilon \quad (\text{Abbey, 2016}) \quad (3)$$

Where

σ = *Stress of the entire bar element, Pa*

E = *Young Modulus of the bar element, Pa*

ε = *strain of the bar element*

Thus the stresses and strains for a group of elements that made up the meshed 3D structure can be calculated using computers to generate FEA results.

A lower extremity exoskeleton named as Soldier Lower Extremity Exoskeleton (SLEE) is created based on the movements of a soldier that is meant for load carrying (Zhao, et al., 2013). A three-dimensional model of this exoskeleton is modelled in Unigraphics as a virtual prototype to validate the rationality of its design and to conduct kinematics and dynamics simulation. The FEA model however which is the simplified version of the virtual prototype was created in ANSYS to conduct the FEA simulation with the intent to optimize this exoskeleton. Some but not all of the components of the FEA model are simplified (Zhao, et al., 2013).

2.6 Human Isometric Strength

The human isometric strength abbreviated as HIS of a human arm is the measure of strength where the human's arm could no longer move (Naidu, 2011). Figure 2.6 shows the human arm's degree of freedom while Table 1 shows the human isometric strength. Referring to Figure 2.6 and Table 1, the shoulder movement has torque values of 110Nm and 125Nm. Because $125\text{Nm} > 110\text{Nm}$, the shoulder or upper arm's torque of the proposed exoskeleton is taken as 125Nm. The elbow's torque for the proposed exoskeleton however is taken as 72.5Nm while the forearm twisting motion's torque is taken as 9.1Nm.

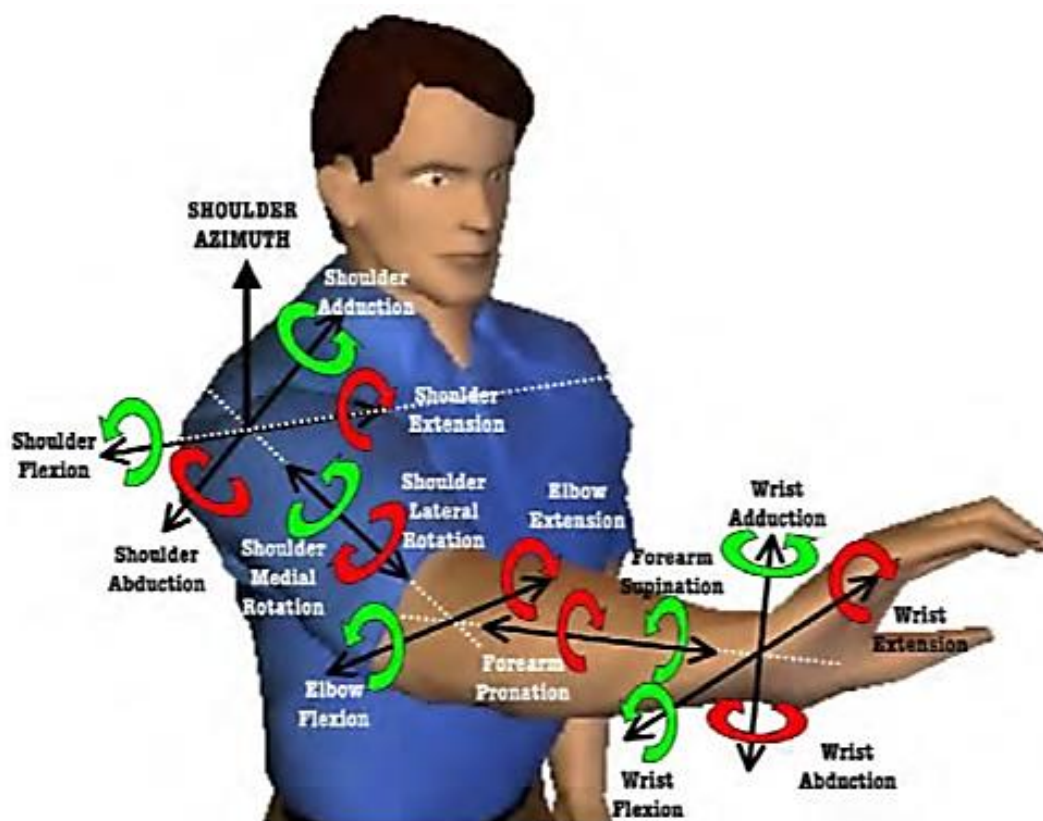


Figure 2.6 Human Arm Degree of Freedom (Carignan and Liszka, 2005 cited in Naidu, 2011).

Table 1: Human Isometric Strength (Tsagarakis, Caldwell, and Medrano-Cerda, 1999 cited in Naidu, 2011)

DOF		Torque (Nm)
Shoulder	Flexion/Extension	110
	Abduction/Adduction	125
	Medial/Lateral Rotation	-
Elbow	Flexion/Extension	72.5
	Supination/Pronation	9.1

2.7 Summary

The design of exoskeleton shown in Figure 2.1 uses springs to resist the patient's movement. These springs that are attached near the human body could be hazardous if the springs are affected by rust or are improperly attached which could lead to injury.

The use of cables in exoskeletons are tedious to maintain and that these cables could potentially frail at the small cracks that are hard to detect and could potentially cause sudden mechanical failure leading to unwanted injury or death. The design of exoskeletons that uses electromagnetic motors to actuate them may be simple and easy to implement but it requires motors that have high power to weight ratio that can be expensive as compared to conventional motors in the market. The exposure of these motors and life wiring at the links and joints can also be hazardous if it comes into contact with liquids or if accidental collision from other people occurs.

The use of pneumatic pistons to actuate the exoskeleton has issues with leakages and they risk the patient to be near heavy and pressurised reservoirs. These problems that occur from the usage of pneumatic pistons are also similar to that of hydraulic pistons in general.

Thus there is a need to improve the existing exoskeleton designs mentioned in literature by designing a new exoskeleton design. The research gap of this study is to develop an exoskeleton that is capable of transmitting the input torque mechanically from the base to the limbs without the use of cables, pneumatic and hydraulic piston. This is done with the use of mechanical systems such as rack and pinion mechanisms, cams and linkages.

Section 2.5 of the report shows the basic understandings of the finite element method that is possibly used by computers to perform the FEA simulation. Section 2.6 of the report however shows the torque measurements of the human isometric strength that the proposed exoskeleton will be subjected to during the FEA simulation.

The method to select several components from an exoskeleton for the FEA simulation that is used in this study is similar to Zhao, et al.,'s (2013) paper. This method will be discuss in detail in section 3.1 of the report as well as the differences between the method used in this study and the method used by Zhao, et al.,'s (2013) paper.

CHAPTER 3

METHODOLOGY

3.1 Workflow

This section of the report elaborates on the research method used in this study and is graphically summarised in Figure 3.1.

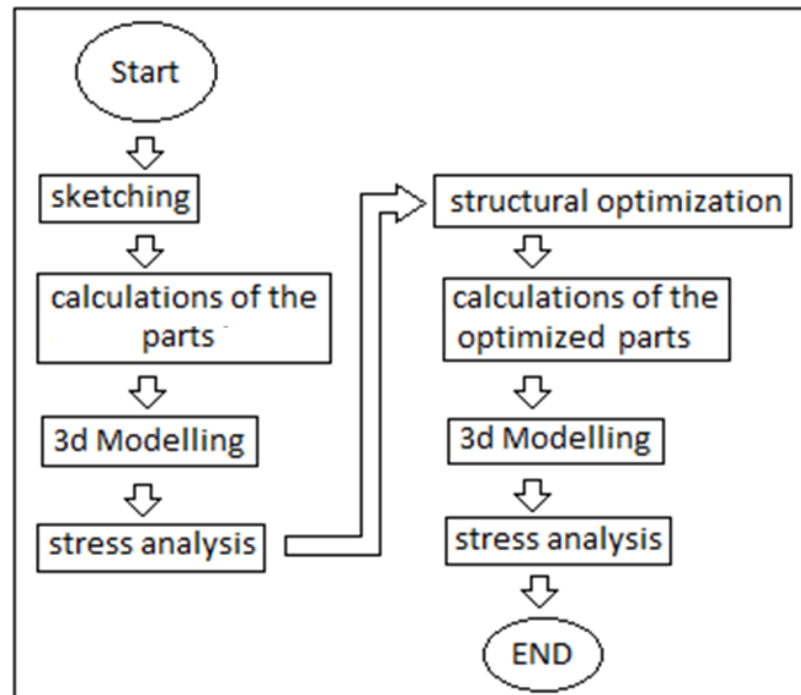


Figure 3.1 Research Cycle

The research cycle briefly describes that the proposed exoskeleton was sketched before the chosen parts of this device were calculated and modelled in Solidworks, undergoes structural analysis and, were structurally optimized. The optimized parts were then recalculated, modelled and, the structural analysis process was carried out for these parts. Thus the proposed mechanical based exoskeleton was not only developed but is also optimized to reduce material usage.

As mentioned in section 2.7 of the report, the method to simulate only selected parts of an exoskeleton that is used in this study is similar to the method used in Zhao, et al.,'s (2013) paper. However, the parts of the proposed exoskeleton was simulated individually while Zhao, et al., (2013) exoskeleton's components were simplified, assembled and simulated as a whole three-dimensional structure. Zhao, et al.,'s (2013) paper discuss on the optimization of a gait exoskeleton while this study is focused on optimizing an upper extremity exoskeleton.

To begin the research method of this study, the entire structure of the exoskeleton and its working principals were sketched in the software; Blender. This software was meant to provide a quick and rough estimate of the part's geometry and dimensions to aid in the brainstorming process when developing the mechanical principals and the overall structure of the proposed exoskeleton. The parts of this exoskeleton were later remodelled in solidworks accurately.

A selected number of the newly designed exoskeleton's parts were then calculated to determine the minimum dimensions needed to withstand the maximum allowable stress. The deflections of these parts except the upper arm were also calculated to withstand the maximum allowable deflection. The upperarm part is to be duplicated to add support to the exoskeleton's structure whenever necessary. Such implementation will consequently reduce the deflection of the multiple upperarm parts used to stabilize the fore mentioned structure. Optimizing a single upperarm beam and duplicating it is the preferred method to optimize the upper arm part to reduce its material usage.

The stress analysis was performed by applying loads and constraints onto the 3D models before running the FEA simulation. The results obtained from the simulation were recorded and used to identify the high stress areas of the parts. These areas that were projected from the FEA results were used as an insight to develop the optimized parts.

The optimized design was then brainstormed with the use of trusses and hollow cylinders for the parts. Trusses exist everywhere in bridges and structures all over the world and have shown their capability to support heavy loads with minimal material usage. These parts were also calculated to determine the minimum dimensions needed to withstand the fore mentioned maximum allowable stress. Not all of the optimized parts were calculated to withstand the maximum allowable deflection. These parts including the upperarm were made of trusses and that their deflections relied on raw simulation alone. This is due to the dimensions of the individual beams capable of being manipulated to be slightly larger than the intended value to make the whole truss structure stiffer and possibly stronger than intended. However, care must be taken when adding more materials to the optimized parts so as to avoid making the optimized parts heavier than the un-optimized parts.

The optimized parts were then remodelled and the stress analysis was carried out. The FEA results produced from the simulation of the optimized parts were recorded. A conclusion was then drawn to end the research cycle.

Although errors were made during calculation for both the optimized and un-optimized versions of Part B and the forearm, these errors resulted in the parts being overdesigned to be larger than their intended dimensions to have higher structural strength. These errors were mention in detail alongside their calculation in later sections of the report.

Stress singularity issues are unavoidable software errors that concentrate around the bolt hole areas (Kurowski and Dvorak,2011) of the lowerarm and Part B. The mesh of the bolt hole areas are small and the finer the mesh size of these holes, the higher the stress value that is concentrated at these bolt hole areas (Kurowski and Dvorak, 2011). Increasing the bolt hole sizes however reduces the stress acting on

these holes but this does not reflect on an actual real life scenario. To solve the problem of the stress singularity, this problem is globally ignored by taking the stress areas that is sufficiently far away from it even though this could inevitably affect the accuracy of the reading (Walter, 2013). Thus it is important to have supporting calculations to validate the part's structural theory.

CHAPTER 4

RESULTS AND DISCUSSION

4.1 Overview

The proposed exoskeleton was sketched in blender and the working principals presented. Calculations were made to determine the part's minimal dimensions needed to withstand the targeted stress and deflections before these parts were modelled and simulated in Solidworks. The deflection of the upper arm is controlled by its duplication and positioning and not by the calculation of its minimum dimensions needed to withstand the targeted deflection. Figure 4.11 shows that the upperarm has been duplicated into 2 parts and the further these parts are from each other, the lesser the moment forces will act on these parts leading to a decrease in deflection and possibly stresses. However more upperarm parts may be needed whenever necessary to ensure the safety of this device but such implementation is reserved for future research. The results obtained from the FEA simulation provides a design insight to aid in the development of the optimized model. The optimized parts were then calculated to determine the part's minimal dimensions to withstand the targeted stress. The part's minimal dimensions to withstand the targeted deflections however are either calculated or relied on the slight mass increase of its detailed geometry. The newly optimized parts are then modelled and simulated in Solidworks and the FEA results produced. A part was considered functional if its results were within the maximum allowable yield stress, and deflections. Finally the results were discussed in the discussion section of the report and a conclusion was made to describe the significant changes that have occurred after optimization of the exoskeleton's parts.

4.2 Working Principle of Exoskeleton

Figure 4.1 shows the proposed exoskeleton while Figure 4.2 and Figure 4.3 shows its range of motion. The proposed exoskeleton has two parallelograms where the Upper arm, part B, C and D forms the parallelogram 2 and the Upper arm, Lower arm, Part E and F forms the parallelogram 1.

Paralelogram1 and parallelogram 2 are mechanical actuators that were chosen to be optimized in this study.

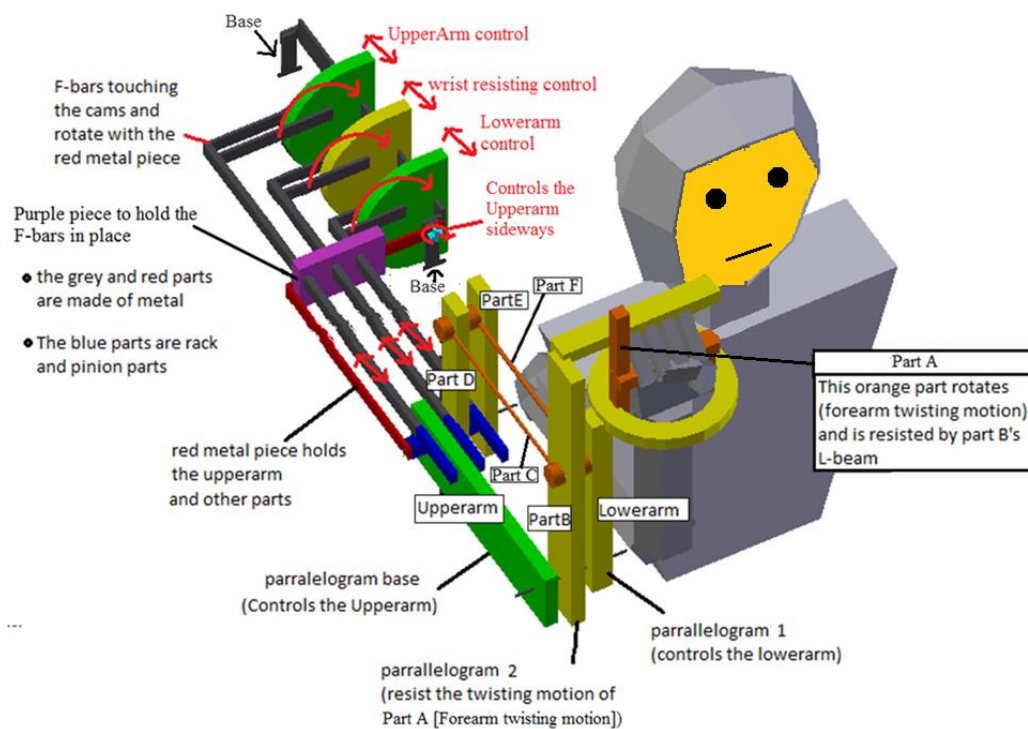


Figure 4.1 Proposed Exoskeleton

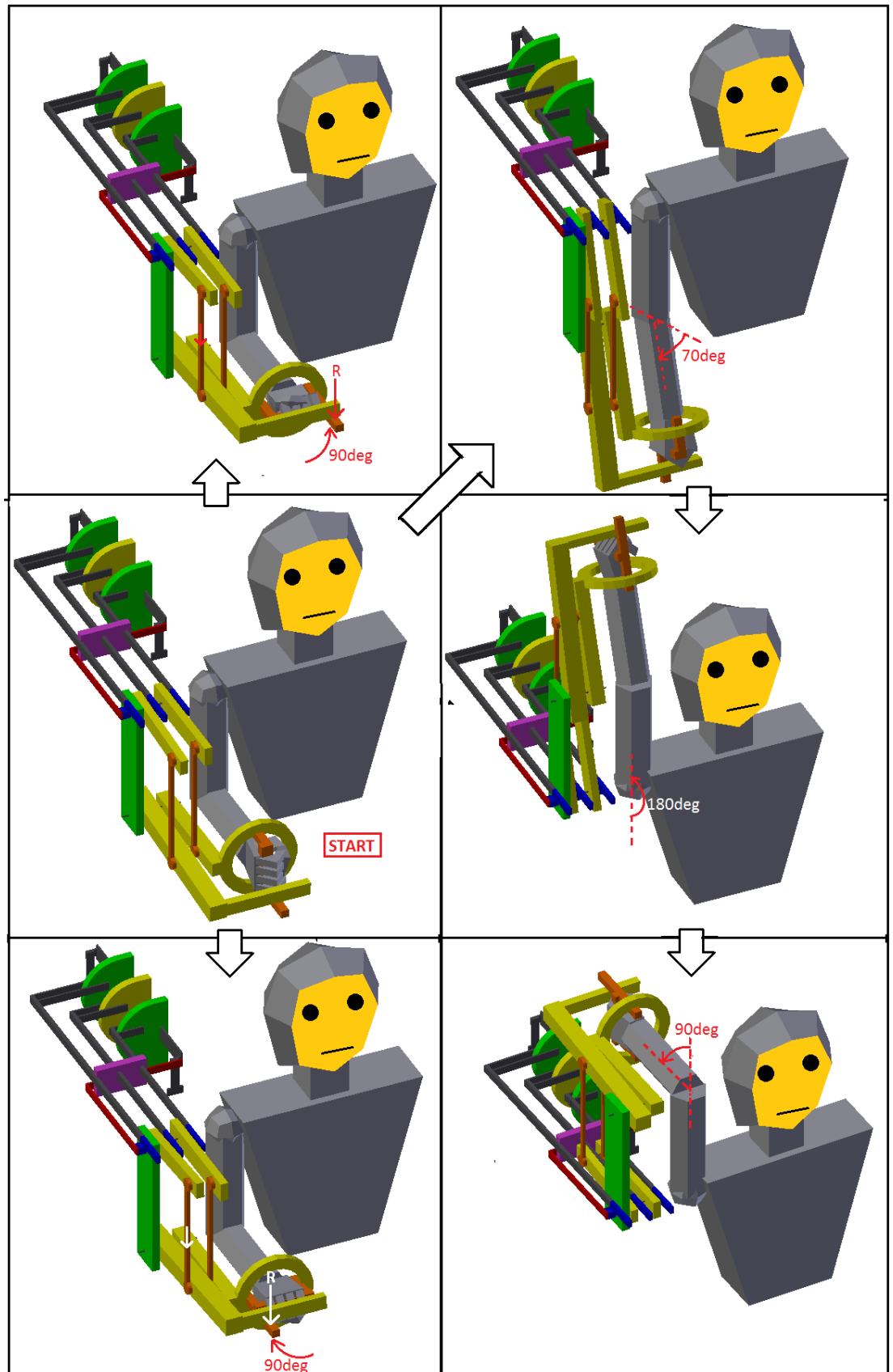


Figure 4.2 Proposed Exoskeleton Range of Motion 1

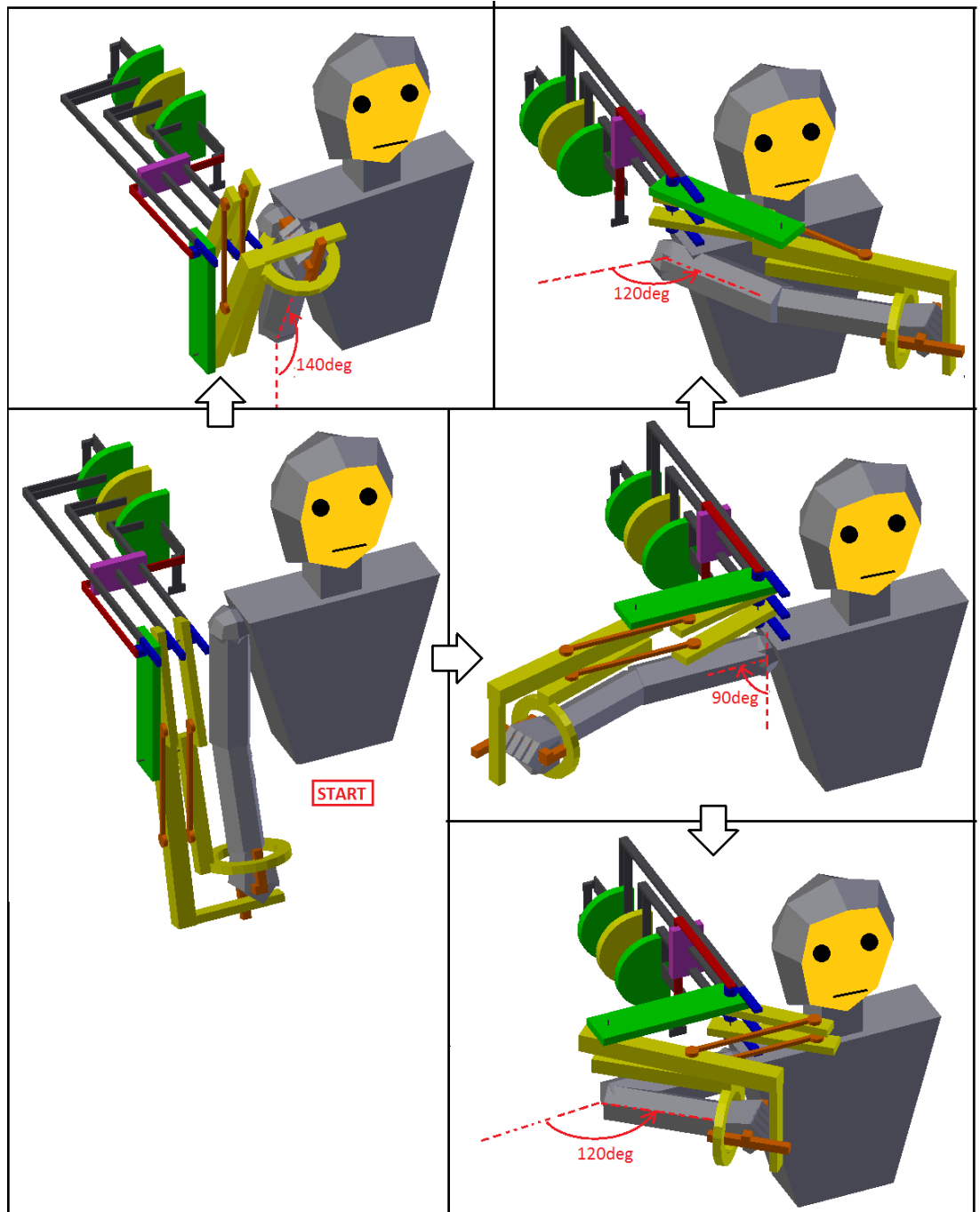


Figure 4.3 Proposed Exoskeleton Range of Motion 2

The input of this mechanical system begins at the green and yellow semi-circular cams that are expected to be controlled by linear actuators. The cyan piece in Figure 4.1 however is not part of the exoskeleton's entire structure but it is an indicator

showing the input location of a rotational actuator needed to be connected to the red metal piece responsible for the upper arm's sideways rotation of the exoskeleton.

The cams control the linear movements of the metallic F-bars touching them and are coloured in grey. The purple piece that is attached to the red metal piece is meant to constraint these F-bars onto the red metal piece. As the red metal piece rotates, the F-bars rotates with it along its axis of rotation.

The end of the metallic F-bars are connected to the rack and pinion mechanisms coloured in blue. A blue cylinder is used to represent a pinion gear while a blue bar is used to represent a rack. These pinions are attached to the upperarm, Part D and Part E.

The upperarm provides the front facing up and down movements of the exoskeleton. Part D controls Parallelogram2 while Part E controls Parallelogram1. Parallelogram1 controls the elbow motion of the exoskeleton while part A is meant for the user to apply a twisting motion from the user's forearm. Parallelogram2 then resist the twisting motion exerted from part A at part B's L-beam.

Referring to Figure 4.1, the parts chosen to be calculated and optimized are the lowerarm, the upperarm, Part B, D and E. Part C and F from parallelogram2 and parallelogram1 respectively are bars where each of them has only 2 equal forces acting at their ends and are perpendicular to their respective cross section (Myszka, 2005). These forces results in Part C and F to be subjected to tensile stresses only and that changing their geometrical shapes with the intent to optimize them may not be possible due to the formula;

$$\sigma = \frac{F}{A} \quad (4)$$

Where

σ = tensile stress of these links, Pa

F = forces acting along the cross section of these links , N

A = cross sectional area of the links, m^2

Part A is not chosen to be optimized as it was viewed separately from the mechanical actuators of parallelogram2 and parallelogram1. Thus Part A was not chosen to be optimized in this study but its optimization is reserved for future research. Figure 4.4 shows Part A that will be used to aid in the calculations presented in later sections of the report

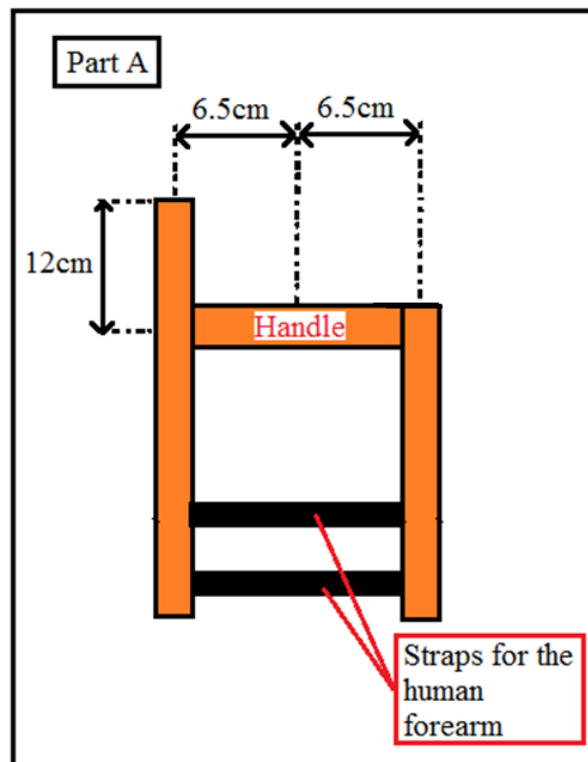


Figure 4.4 Part A

4.3 Solidworks settings

The 3D model of the exoskeleton's parts is imagined to be made of PLA. PLA is a 3D printing plastic material that has a tensile strength of up to 50MPa (Shuvom, 2015) making it a decently strong material. The yield stress of PLA is also near 50MPa (Farsetti, et al., 2011). Thus the yield stress for PLA is assumed to be 50MPa.

According to Juvinal and Marshek (2000) the safety factor for the parts are taken as:

$$\text{safety factor} = \frac{\text{strength of the material}}{\text{Stress due to actual load}} \quad (5)$$

A safety factor of 2.5 is the minimum number for a less tried material subjected to normal environmental conditions, stresses and loads (Juvinal and Marshek, 2000) Thus using the safety factor formula from Juvinal and Marshek (2000) the stress due to actual load is calculated as

$$\frac{\text{Strength of material}}{\text{safety factor}} = \frac{50}{2.5} = 20MPa \quad (6)$$

Pandhare, et al.,'s (2014) paper uses a maximum allowable deflection of 2.5mm for general practice in the design of a skid base frame. Thus the general practice of the maximum allowable deflection used in this study is the same as the maximum allowable deflection used in Pandhare, et al.,'s (2014) paper with a value of 2.5mm.

The density, shear modulus and young modulus for PLA are 1.3g/cm³, 2.4GPa and 3.5GPa respectively (MakeItFrom.com, 2016). The Poisson ratio for PLA however is 0.024 (Amy, 2012). These material properties of PLA are used in the Solidworks simulation (DassaultSystèmes, 1995-2016).

4.4 Overview of Calculation of the Exoskeleton's Parts

Unless specified, the formulas used to calculate the moment of inertia 'I' and the polar moment of inertia 'J' presented in the entire section 4.4 of this report were taken from Ugural (2008) and Tigerquest.com (2016) respectively. The load, shear and moment diagrams were learnt from Ugural (2008) The stress formulas are taken from Ugural (2008) while the deflection formulas are taken from Pytel and Kiusalaas (2012). The moment of inertia 'I' for a rectangular beam according to Ugural (2008) is;

$$I = \frac{bh^3}{12} \quad (7)$$

The polar moment of inertia 'J' for a rectangular beam according to Tigerquest.com (2016) is;

$$J = \frac{bh(b^2+h^2)}{12} \quad (8)$$

Where;

I =moment of inertia, m^4

J = polar moment of inertia, m^4

b = width of a rectangular cross section, m

h = height of a rectangular cross section, m

As mentioned in section 4.3 of the report, the maximum allowable yield stress and deflections is currently 20MPa and 2.5mm respectively while the young modulus of the material imagined to be used in the parts is 3.5GPa

The procedure to calculate the developed exoskeleton's parts described in this section of the report applies to only section 4.4, and 4.7 of the report

To begin calculation of the chosen parts of the proposed exoskeleton, the cross sections of these parts are intuitively determined. These cross sections are viewed as imaginary cantilever beams subjected to stresses.

Part D and E from Figure 4.1 are simple cantilever beams with only one force applied at its end. Thus the calculations are predictably simple and no free body diagrams are needed to identify the maximum moment of these parts.

The Upper arm part, fore arm part, and Part B calculations however are complex as there are several forces acting upon these parts. Thus there is a need to identify the maximum moment or the highest force acting on a particular cross section sampled from these parts. These sampled cross sections are viewed as imaginary cantilever beams for ease of calculation. Free body diagrams of these imaginary beams are drawn to calculate and find the forces acting on it including the maximum force acting on these beams. The load, shear and moment diagrams learnt from Ugural (2008) are then drawn to identify the maximum moment acting on these beams.

After the highest moments or forces of the chosen cross sections are identified, the stress formulas learnt from Ugural (2008) are used to calculate the parts with the intent to produce the minimum dimensions required to withstand the allowable stress limit. These dimensions could be either the width 'b' or the height 'h' of the chosen cross sections or both.

The Bending stress formula according to Ugural (2008) is given as,

$$\sigma = \frac{My}{I} \quad (9)$$

Where,

$\sigma = stress, Pa$

$M = moment, Nm$

$y = \frac{h}{2}, for a square bracket, m$

$h = height of a rectangular cross section, m$

$I = moment of inertia, m^4$

The tensile/compression stress formula according to Ugural (2008) is given as,

$$\sigma = \frac{F}{A} \quad (10)$$

Where,

$\sigma = stress, Pa$

F= Force, N

A= Area, m^2

If the calculated cross section is subjected to both torsional and bending stresses, then these stresses are used in the principal stress formulas to calculate the minimum and maximum principal stresses(Ugural, 2008). The torsional shear stress formula according to Ugural (2008) is given as,

$$S = \frac{Tr}{J} \quad (11)$$

Where,

$S = Torsional\ shear\ stress, Pa$

r is taken as $\frac{b}{2}$, for a square bracket, m

b = width of a rectangular cross section, m

$J = polar\ moment\ of\ inertia, m^4$

T = torque, Nm

The principal stress formulas according to Ugural (2008) are given as,

$$\sigma_1 = \frac{\sigma_x + \sigma_y}{2} + \sqrt{\left(\frac{\sigma_x - \sigma_y}{2}\right)^2 + S^2} \quad (12)$$

$$\sigma_2 = \frac{\sigma_x + \sigma_y}{2} - \sqrt{\left(\frac{\sigma_x - \sigma_y}{2}\right)^2 + S^2} \quad (13)$$

Where,

σ_1 = maximum principal stress, Pa

σ_2 = minimum principal stress, Pa

σ_x = stress in the x-direction, Pa

σ_y = stress in the y-direction, Pa

If a particular cross section has only one bending stress acting parallel to it then σ_x is taken as the bending stress while σ_y is taken to be zero (Ugural, 2008). The maximum and minimum principal stresses obtained from the principal stress formulas are then used to find the yield strength from the von mises's energy of distortion equation for a plane stress (Ugural, 2008) is given as,

$$\sigma_y^2 = \sigma_1^2 - \sigma_1\sigma_2 + \sigma_2^2 \quad (14)$$

Where,

σ_y = *yield stress*

σ_1 = *maximum principal stress*

σ_2 = *minimum principal stress*

Rearranging equation (14), the yield stress is written as;

$$\sigma_y = \sqrt{\sigma_1^2 - \sigma_1\sigma_2 + \sigma_2^2} \quad (15)$$

Thus the minimum value of a particular dimension needed to withstand the allowable stress limit is calculated and obtained.

After obtaining the dimensions needed to withstand the allowable stress limit, the deflection formulas learnt from Pytel and Kiusalaas (2012) are later used to calculate the parts of the exoskeleton except the upper arm part with the intent to produce the minimum dimensions needed to withstand the allowable deflection limit. These dimensions could be either the width 'b' or the height 'h' for a rectangular cross sections or both. Figure 4.5 shows the deflection formulas

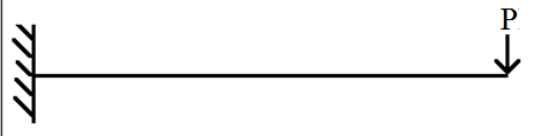
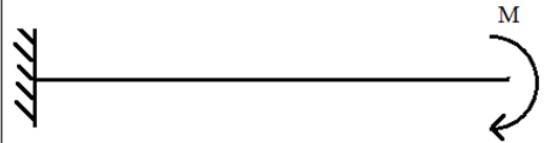
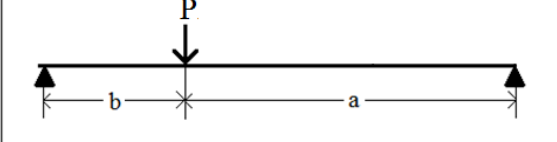
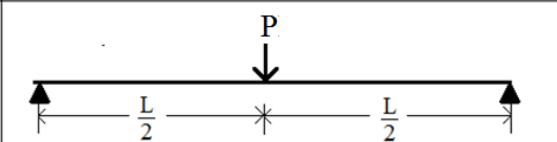
case	Deflection δ
	$\frac{PL^3}{3EI}$
	$\frac{ML^2}{2EI}$
	$\frac{Pb(L^2 - b^2)^{\frac{3}{2}}}{9\sqrt{3}LEI}$
	$\frac{PL^3}{48EI}$

Figure 4.5 Deflection formulas taken from Pytel and Kiusalaas (2012)

Where,

E= Young Modulus, Pa

I=moment of inertia, m^4

L= length of the beam, m

P=force, F

M=moment, Nm

a = length, m

b = length, m

Thus the minimum value of a particular dimension needed to withstand the allowable deflection limit is calculated and obtained.

Finally, this leads to a pair of results that are compared and the value of the calculated dimension that makes the part thicker and heavier is the needed thickness or height to withstand both the allowable yield stress and the allowable deflection limit.

4.4.1 Calculation of the Forearm Part

Figure 4.6 shows the diagrams for the cross section-x of the Fore Arm Part. Figure 4.6 (a) shows the free body diagram for the cross section-x of the Lower arm part. The input torque values of 9.1Nm and 72.5Nm are caused by the forearm's twisting motion and the elbow respectively according to explanations given in section 2.6 of the report. The 72.5Nm and 9.1Nm torques are converted into F_1 and F_2 respectively.

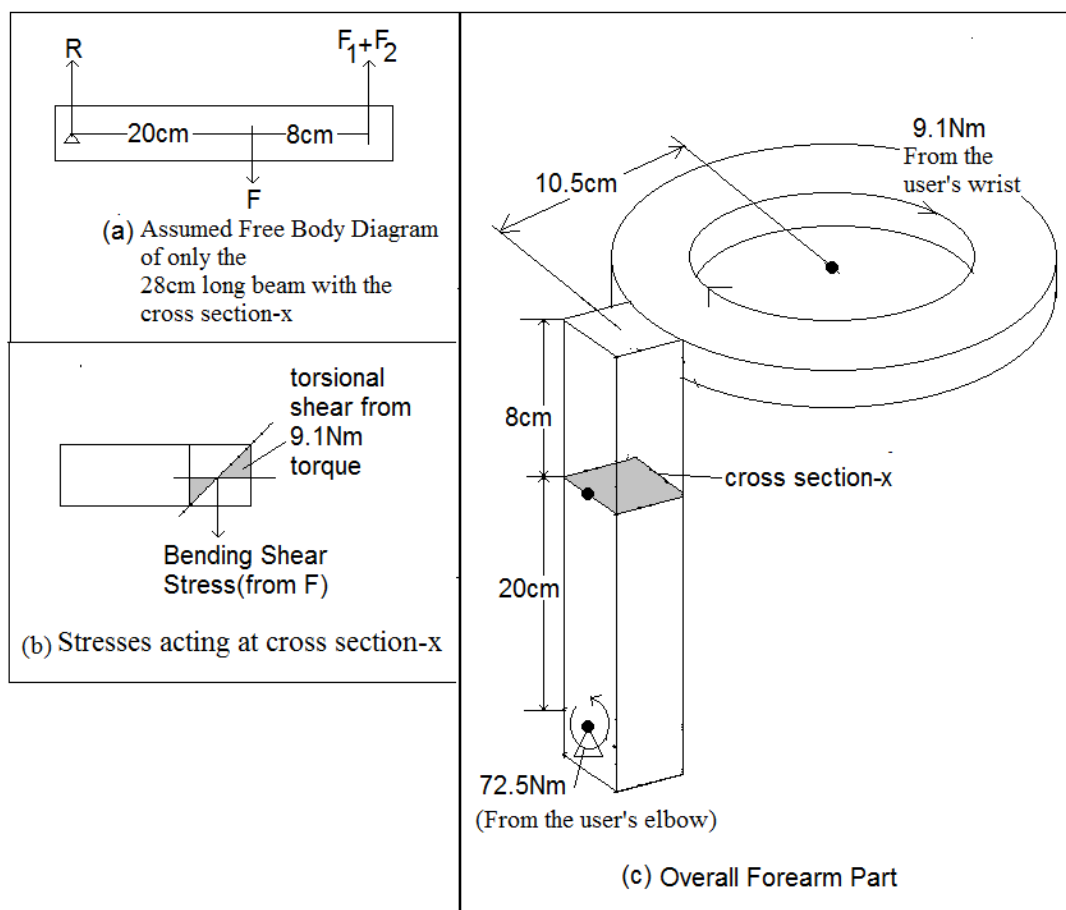


Figure 4.6 Diagrams for the cross section-x of the Fore Arm Part. Diagram (b) is generated according to theory given by Learn Easy (2013)

Converting the 9.1Nm torque into F_2

$$F_2 = \frac{9.1}{0.105} = 86.67N$$

Converting the 72.5Nm torque into F_1

$$F_1 = \frac{72.5}{0.28} = 258.93N$$

$$\Sigma M \text{ at } R = 0, \quad -F(0.2) + (F_1 + F_2)(0.28) = 0$$

$$F=483.83N$$

$$\Sigma F = 0, \quad R - F + F_1 + F_2 = 0$$

$$R=138.24N$$

The reaction force $R=138.24N$ will act upon a long screw held by the upper arm part as shown in Figure 4.11. The load, shear and moment diagrams that are learnt from Ugural (2008) are drawn for the cross section-x for the forearm and is shown in Figure 4.7.

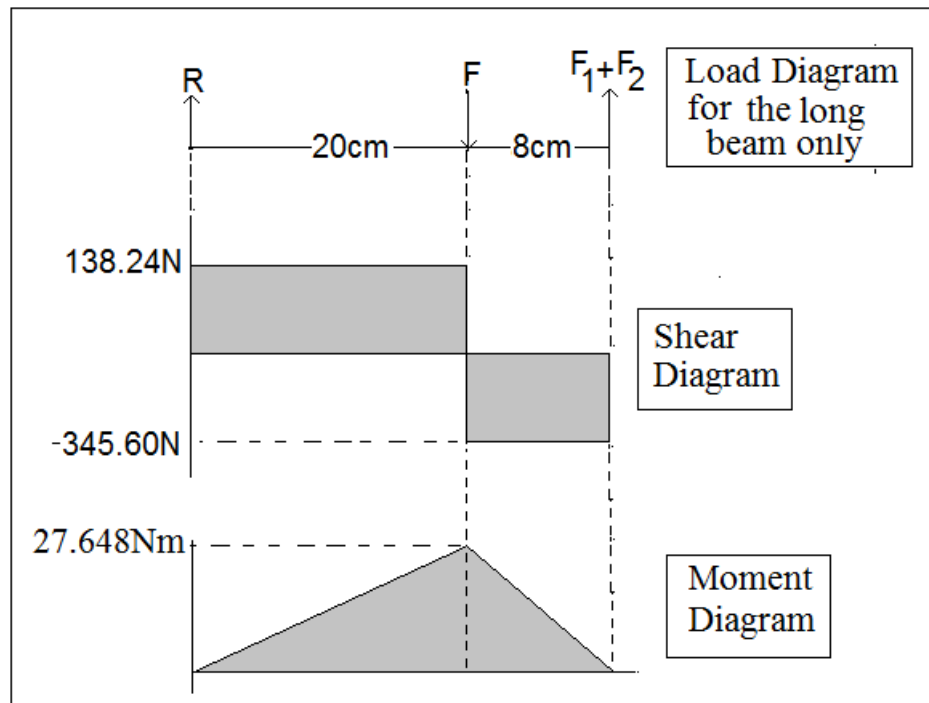


Figure 4.7 Load, Shear and Moment Diagram for cross section-x of the forearm

Thus from Figure 4.7, the maximum moment is 27.648Nm. Unfortunately, errors were made and the moment was taken as 96.766Nm to calculate the model's dimensions. This error results in the forearm part being oversized to have a larger dimension that will increase the strength of the structure. Moreover, the optimized forearm part calculated in section 4.7.1 of the report was also designed based on this error making it larger but stronger. Thus both the un-optimized and optimized forearm parts are credibly comparable.

The forearm part at cross section-x is viewed as a beam undergoing combine stresses. Calculating the dimension of width 'b' for the cross section-x needed to withstand the allowable stress of 20MPa using the stress formulas available in section 4.4 of the report;

Setting b=h for both cross sections x and y,

$$\text{Bending Stress } \sigma = \frac{My}{I} = \frac{(96.766)\left(\frac{b}{2}\right)}{\frac{b^4}{12}} = \frac{580.6}{b^3}$$

$$\text{Torsional Shear Stress } S = \frac{Tr}{J} = \frac{9.1\left(\frac{b}{2}\right)}{\frac{b^4}{6}} = \frac{27.3}{b^3}$$

$$\text{The maximum principal stress } \sigma_1 = \frac{\sigma_x + \sigma_y}{2} + \sqrt{\left(\frac{\sigma_x + \sigma_y}{2}\right)^2 + s^2}$$

$$= \frac{\frac{580.6}{b^3} + 0}{2} + \sqrt{\left(\frac{\frac{580.6}{b^3} + 0}{2}\right)^2 + \left(\frac{27.3}{b^3}\right)^2} = \frac{581.88}{b^3}$$

$$\text{The minimum principal stress } \sigma_2 = \frac{\sigma_x + \sigma_y}{2} - \sqrt{\left(\frac{\sigma_x + \sigma_y}{2}\right)^2 + s^2}$$

$$= \frac{\frac{580.6}{b^3} + 0}{2} - \sqrt{\left(\frac{\frac{580.6}{b^3} + 0}{2}\right)^2 + \left(\frac{27.3}{b^3}\right)^2} = -\frac{1.28}{b^3}$$

$$\text{The yield stress } \sigma_y = \sqrt{\sigma_1^2 - \sigma_1\sigma_2 + \sigma_2^2}$$

$$= \frac{582.5223}{b^3} = 20MPa$$

$$b = 0.0307 \approx \mathbf{3.1cm}$$

Calculating the dimension of width b for the cross section-x needed to withstand the allowable deflection of 2.5mm using the deflection formulas available in Figure 4.5. The deflections are intuitively assumed to be;

$$\begin{aligned}\delta_{total} &= \delta_{bending} + \delta_{torsion} \\ &= \frac{Pb(L^2 - b^2)^{\frac{3}{2}}}{9\sqrt{3}LEI} + \frac{ML^2}{2EI} \\ &= \frac{(483.83)(0.08)(0.28^2 - 0.08^2)^{\frac{3}{2}}}{9\sqrt{3}(0.28)(E)\left(\frac{b^4}{12}\right)} + \frac{9.1(0.105)^2}{2(E)\left(\frac{b^4}{12}\right)} = 0.0025mm\end{aligned}$$

$$\text{For } E = 3.5GPa, b = 0.02335 \approx \mathbf{2.4cm}$$

The calculation results for width- b are compared for the cross section-x

3.1cm > 2.4cm, thus the width 'b' and height 'h' of the square cross section-x for the fore arm part is taken to be 3.1cm to ensure that the forearm part at this cross section does not exceed both the allowable yield stress and allowable deflection. However as mentioned before, the error of the maximum moment value has caused the un-optimized and optimized parts of the forearm to be larger than the intended dimensions but this adds to both of these structures' strength.

Figure 4.8 shows the diagrams for the cross section-y of the Fore Arm Part. The cross section Y and the entire adjacent ring is assumed to function as a cantilever beam and its free body diagram is shown in Figure 4.8(b)

Combining the 72.5Nm and 9.1Nm torque

$$F = \frac{9.1}{0.105} + \frac{72.5}{0.28} = 345.60N$$

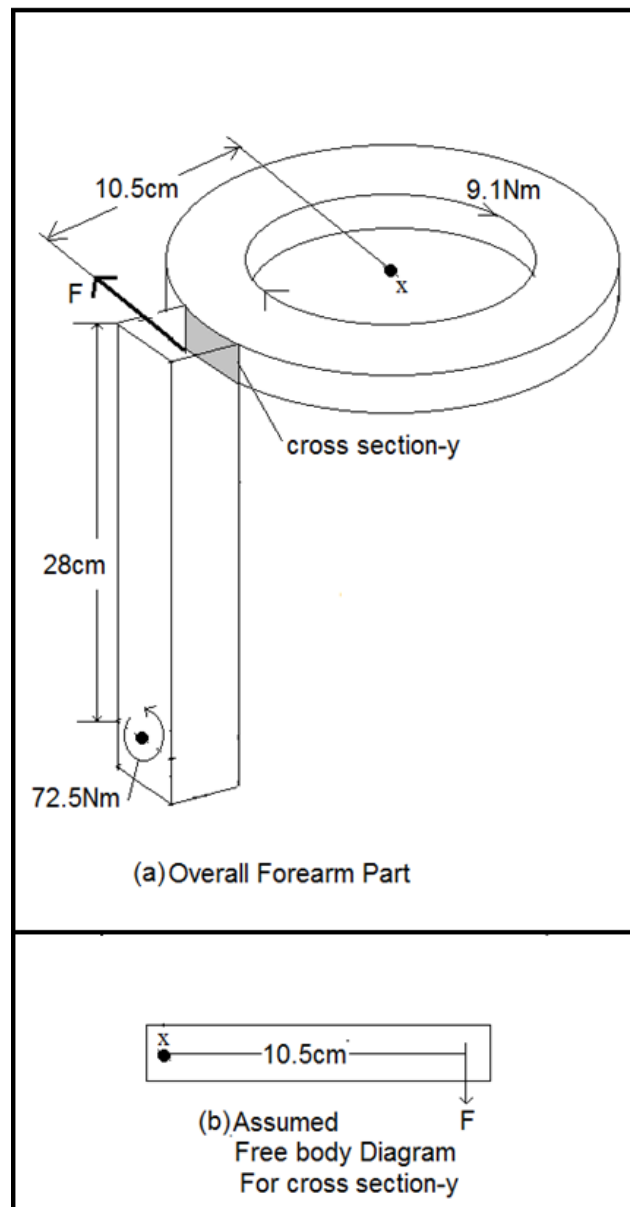


Figure 4.8 Diagrams for the cross section-Y of the Fore Arm Part

The width 'b' was set to 1.8cm to match with the width of the forearm's ring's cross sectional area that was calculated to be 1.8cm and will be explained near the end of section 4.4.1 of the report. This width also called as 'thickness' has also been used for the optimized forearm part.

Calculating the dimension of height 'h' for the cross section-y needed to withstand the allowable stress of 20MPa using the stress formulas available in section 4.4 of the report.

$$\sigma = \frac{My}{I} = \frac{(345.60)(0.105) \left(\frac{h}{2}\right)}{\frac{0.018 \times h^3}{12}} = 20MPa$$

$$b = 0.0246 \approx \mathbf{2.5cm}$$

Calculating the dimension of height 'h' for the cross section-y needed to withstand the allowable deflection of 2.5mm using the deflection formulas available in Figure 4.5

$$\delta = \frac{FL^3}{3EI} = \frac{(345.60)(0.105)^3}{3(E) \left(\frac{0.018 \times h^3}{12}\right)} = 0.0025$$

$$\text{For } E=3.5GPa, b=0.0217 \approx \mathbf{2.2cm}$$

Comparing the height 'h' calculation results for the cross section-y

2.5cm > 2.2cm. However, it is preferable for the height 'h' to be 3.1 cm to match with the previously calculated cross section-x of the forearm part's square beam of 3.1 x 3.1 cm^2 . Thus the width 'b' and the height 'h' of the square cross section-y for the fore arm part is taken to be 1.8 cm and 3.1cm respectively to ensure that the forearm part at this cross section does not exceed both the allowable yield stress and allowable deflection. Unfortunately, errors were made and the height 'h' was slightly increased to 3.6cm. A solid piece with an estimated cross section of 0.036 x 0.036 m^2 and a thickness of 1.8cm was then modelled and is connected to the end of a 3.1 x 3.1 cm^2 square beam and the forearm's ring at cross section-y. This solid piece has a thickness of 1.8cm and is responsible for joining the un-optimized forearm's ring and its square beam. The cross sectional area for this solid piece is

$$0.036 \times 0.036 = 1.296 \times 10^{-3} m^2$$

The hollow cylinder for the optimized forearm part has a solid cylinder at its end connecting to the adjacent optimized forearm's ring. This solid cylinder has a thickness of 1.8cm and is responsible for joining the optimized forearm's ring and its hollow cylinder. The diameter of this cylinder is 5.8cm which is also the outer diameter of the hollow cylinder calculated from section 4.7.1 of the report. The cross sectional area for half of this solid cylinder is

$$\pi \times \frac{0.058^2}{4} \times \frac{1}{2} = 1.32 \times 10^{-3} m^2$$

$1.32 \times 10^{-3} m^2 \approx 1.296 \times 10^{-3} m^2$. This means the optimized forearm part's solid cylinder is slightly larger when compared to the un-optimized forearm part's solid piece. The optimized forearm part has a lower weight when compared to its un-optimized counterpart shown in Table 2

The ring's cross sectional area however is assumed to be a single cantilever beam that is split into 2 separate beams. Thus the 345.6N force acting on the ring was taken as half for each beam. Calculating the dimension of width 'b' for the ring's cross sectional area needed to withstand the allowable stress of 20MPa using the stress formulas available in section 4.4 of the report

$$\sigma = \frac{My}{I} = \frac{\left(\frac{345.60}{2}\right) (0.105) \left(\frac{b}{2}\right)}{\frac{b^4}{12}} = 20MPa$$

$$b = 0.0176 \approx \mathbf{1.8cm}$$

Calculating the dimension of width b for the ring's cross sectional area needed to withstand the allowable deflection of 2.5mm using the deflection formulas available in Figure 4.5

$$\delta = \frac{FL^3}{3EI} = \frac{\left(\frac{345.60}{2}\right)(0.105)^3}{3(E)\left(\frac{b^4}{12}\right)} = 0.0025$$

For $E=3.5\text{GPa}$, $b=0.0174 \approx \mathbf{1.8\text{cm}}$

Comparing the width 'b' calculation results for cross section-y

1.8cm > 1.8cm. Thus the width 'b' and the height 'h' of the fore arm's ring's cross sectional area is taken to be 1.8cm to ensure that the forearm part at this cross section does not exceed both the allowable yield stress and allowable deflection. This fore arm ring with its $1.8 \times 1.8 \text{ cm}^2$ cross section has also been reused in the optimized forearm part

4.4.2 Calculation for Part B

Figure 4.9 shows the diagrams for part B. In this figure, the cross section x-x undergoes bending and torsional stress. Figure 4.9 (a) shows the free body diagram for the cross section x-x and the cross section y-y.

The 24cm beam of cross-section y-y was design to be longer than intentioned with its end applied with a fixed force F_1 . The reason for such a design was to anticipate the design error due to the lack of distances between the lowerarm part, part B and part F from Figure 4.1 and was explained in section 4.4.5 of the report. This 24cm beam of cross-section y-y for part B has also been reused for its optimized counterpart.

$$F_1 \text{ from part A in Figure 4.4} = \frac{9.1}{0.065} = 140N$$

$$\Sigma M = 0, \quad F_1 \times 0.4 - F_2 \times 0.2 = 0$$

$$F_2 = 2F_1 = 280N$$

$$\Sigma F = 0, \quad F_1 + R - F_2 = 0$$

$$R = 140N$$

The reaction force $R=140N$ will act upon a long screw held by the upper arm part as shown in Figure 4.11

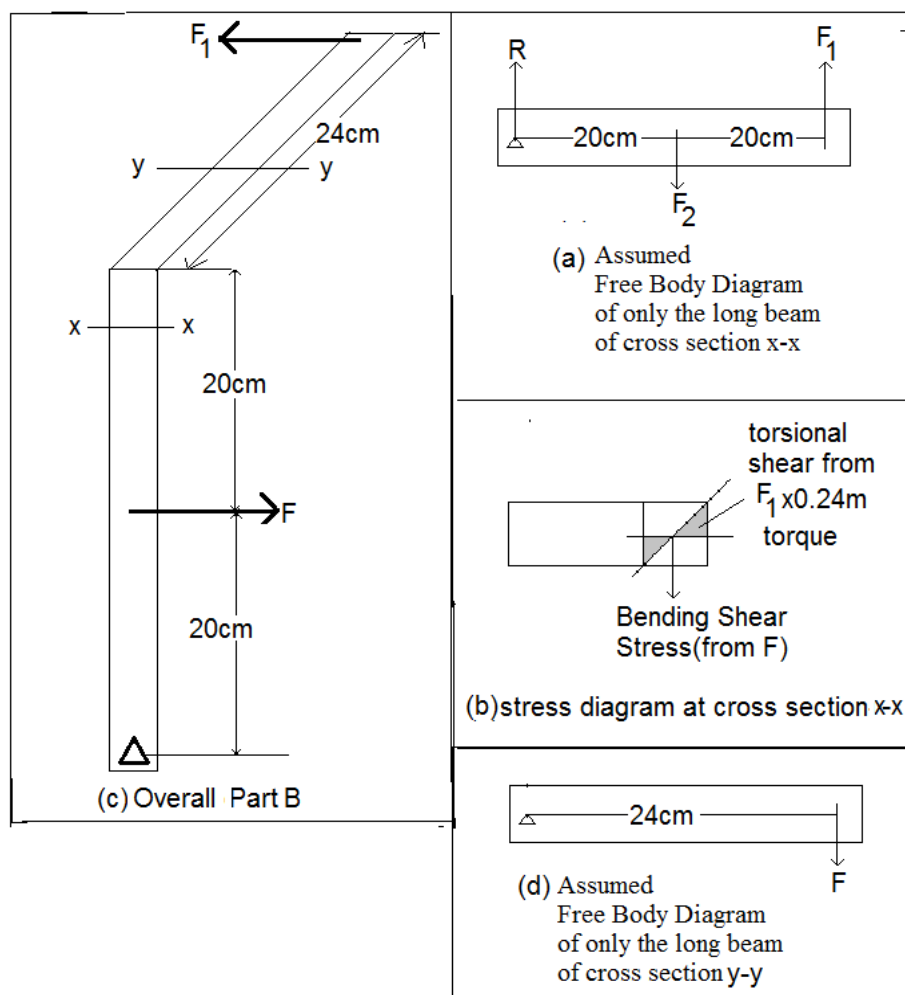


Figure 4.9 Diagrams for Part B. Diagram (b) is generated according to theory given by Learn Easy (2013)

The load, shear and moment diagrams that are learnt from Ugural (2008) are drawn for the cross section-x of the forearm and is shown in Figure 4.10

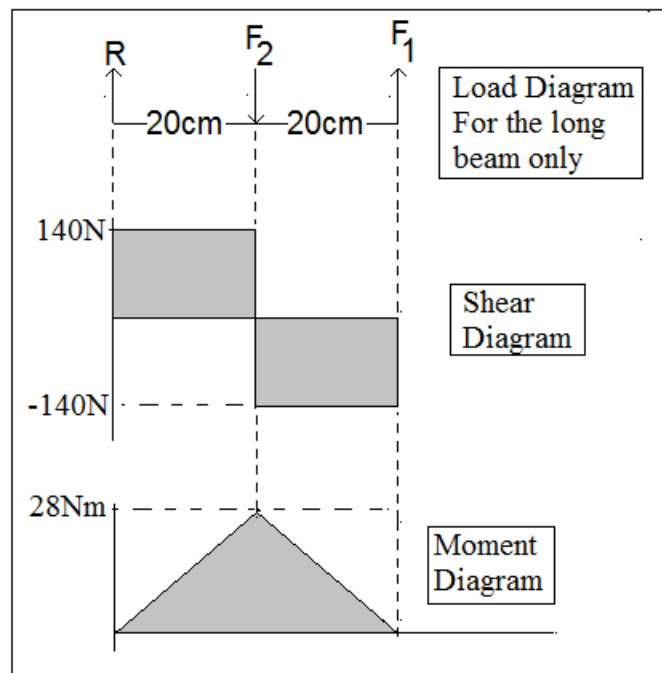


Figure 4.10 Load, Moment, Shear Diagram for the cross section x-x of Part B

Thus from Figure 4.10, the maximum moment is 28Nm. Unfortunately, errors were made and the moment was taken as 48Nm to calculate the model's dimensions. This error results in part B being overdesigned to have a larger dimension that will increase the strength of the structure. Moreover, the optimized part B calculated in section 4.7.2 of the report was also designed based on this error making it larger but stronger.

Further errors were made in the calculations of the optimized Part B that resulted in this part using more material than intended. Thus the cross sectional areas for both the optimized and un-optimized parts are calculated and compared in section 4.7.2 to check and conform the credibility of the optimization process

Calculating the dimension of width 'b' for the cross section x-x needed to withstand the allowable stress of 20MPa using the stress formulas available in section 4.4 of the report

Setting $b=h$

$$\text{Bending Stress } \sigma = \frac{My}{I} = \frac{(48)\left(\frac{b}{2}\right)}{\frac{b^4}{12}} = \frac{288}{b^3}$$

$$\text{Torsional Shear Stress } S = \frac{Tr}{J} = \frac{(140)(0.24)\left(\frac{b}{2}\right)}{\frac{b^4}{6}} = 100.8/b^3$$

$$\text{Maximum principal stress } \sigma_1 = \frac{\sigma_x + \sigma_y}{2} + \sqrt{\left(\frac{\sigma_x + \sigma_y}{2}\right)^2 + s^2}$$

$$= \frac{\frac{288}{b^3} + 0}{2} + \sqrt{\left(\frac{\frac{288}{b^3} + 0}{2}\right)^2 + \left(\frac{100.8}{b^3}\right)^2} = \frac{319.774}{b^3}$$

$$\text{Minimum principal stress } \sigma_2 = \frac{\sigma_x + \sigma_y}{2} - \sqrt{\left(\frac{\sigma_x + \sigma_y}{2}\right)^2 + s^2}$$

$$= \frac{\frac{288}{b^3} + 0}{2} - \sqrt{\left(\frac{\frac{288}{b^3} + 0}{2}\right)^2 + \left(\frac{100.8}{b^3}\right)^2} = \frac{31.774}{b^3}$$

$$\text{The yield stress } \sigma_y = \sqrt{\sigma_1^2 - \sigma_1\sigma_2 + \sigma_2^2}$$

$$= \frac{336.78}{b^3} = 20\text{MPa}$$

$$b = 0.02563 \approx \mathbf{2.6cm}$$

Although the dimension of width 'b' = 2.6cm was derived from the error value causing the maximum moment acting on this cross section to be 48Nm, this dimensional value is not used as the later calculations presented in this report supersedes this value.

Calculating the dimension of width 'b' for the cross section-x needed to withstand the allowable deflection of 2.5mm using the deflection formulas available in Figure 4.5

The deflections are intuitively assumed to be

$$\delta_{total} = \delta_{bending} + \delta_{torsion} = \frac{WL^3}{48EI} + \frac{ML^2}{2EI} = 0.0025$$

$$0.0025 = \frac{(280)(0.4)^3}{48(E) \left(\frac{b^4}{12}\right)} + \frac{(140)(0.24)(0.4)^2}{2(E) \left(\frac{b^4}{12}\right)}$$

$$\text{For } E = 3.5\text{GPa}, b = 0.0438 \approx \mathbf{4.4\text{cm}}$$

Comparing the width b calculation results for cross section-x

4.4cm > 2.6cm, thus the width 'b' and the height 'h' of the square cross section x-x for part B is taken to be 4.4cm to ensure that the part at this cross section does not exceed both the allowable yield stress and allowable deflection.

The cross section y-y of the part B is assumed to act as a cantilever beam and its free body diagram is shown in Figure 4.9 (d). For this cross section of part B, the dimensional width 'b' is set to 0.02m and that b≠h

Calculating the dimension of height 'h' for the cross section-y needed to withstand the allowable stress of 20MPa using the stress formulas available in section 4.4 of the report

$$\text{Bending Stress} \quad \sigma = \frac{My}{I} = \frac{(140)(0.24)\left(\frac{h}{2}\right)}{\frac{(0.02)h^3}{12}} = 20MPa$$

$$h=0.0224 \approx \mathbf{2.3cm}$$

Calculating the dimension of height 'h' for the cross section-y needed to withstand the allowable deflection of 2.5mm using the deflection formulas available in Figure 4.5

$$\delta = \frac{FL^3}{3EI} = \frac{(140)(0.24)^3}{3(E)\left(\frac{(0.02)h^3}{12}\right)} = 0.0025$$

$$\text{For } E = 3.5GPa, h=0.0354 \approx \mathbf{3.5cm}$$

Comparing the height 'h' calculation results for the cross section y-y

3.5cm > 2.3cm, thus the height 'h' and the width 'b' of the rectangular cross section y-y for part B is taken to be 3.5 cm and 2cm respectively to ensure that the part at this cross section does not exceed both the allowable yield stress and allowable deflection.

4.4.3 Calculation for Part D

Part D is assumed to be a simple cantilever beam that undergoes bending stress. Calculating the dimension of width b for Part D needed to withstand the allowable stress of 20MPa using the stress formulas available in section 4.4 of the report.

Setting $b = h$,

$$\text{Bending Stress} \quad \sigma = \frac{My}{I} = \frac{(280)(0.2)\left(\frac{h}{2}\right)}{\frac{h^4}{12}} = 20MPa$$

$$h = 0.0256 \approx \mathbf{2.6cm}$$

Calculating the dimension of height 'h' for part D needed to withstand the allowable deflection of 2.5mm using the deflection formulas available from Figure 4.5

Setting $b = 0.02m$, where $b \neq h$,

$$\delta = \frac{FL^3}{3EI} = \frac{(280)(0.2)^3}{3(E)\left(\frac{(0.02)h^3}{12}\right)} = 0.0025$$

$$\text{For } E = 3.5GPa, h = 0.0371 \approx \mathbf{3.7cm}$$

Comparing the height 'h' from the calculation results

3.7cm x 2cm > 2.6cm x 2.6cm, thus the height 'h' and the width 'b' for part D's rectangular cross section is taken to be 3.7 cm and 2cm respectively to ensure that the part at this cross section does not exceed both the allowable yield stress and allowable deflection.

4.4.4 Calculation for Part E

Part E is assumed to be a simple cantilever beam that undergoes bending stress. Calculating the dimension of width 'b' for Part E needed to withstand the allowable stress of 20MPa using the stress formulas available in section 4.4 of the report

Setting $b = 0.02\text{m}$, where $b \neq h$,

$$\text{Bending Stress} \quad \sigma = \frac{My}{I} = \frac{(483.83)(0.2)\left(\frac{h}{2}\right)}{\frac{(0.02)h^3}{12}} = 20\text{MPa}$$

$$h = 0.0381 \approx \mathbf{3.8\text{cm}}$$

Calculating the dimension of width 'b' for part E needed to withstand the allowable Deflection of 2.5mm using the deflection formulas available in Figure 4.5

Setting $b = 0.02\text{m}$, where $b \neq h$,

$$\delta = \frac{FL^3}{3EI} = \frac{(483.83)(0.2)^3}{3(E)\left(\frac{(0.02)h^3}{12}\right)} = 0.0025$$

$$\text{For } E = 3.5\text{GPa}, h = 0.0445 \approx \mathbf{4.5\text{cm}}$$

Comparing the height 'h' from the calculation results

4.5cm > 3.8cm, thus the height 'h' and the width 'b' for part E's rectangular cross section is taken to be 4.5 cm and 3.8cm respectively to ensure that the part at this cross section does not exceed both the allowable yield stress and allowable deflection.

4.4.5 Calculation for the Upper Arm part

Figure 4.11 shows that the upperarm part has been duplicated and uses 2 simple cantilever beams to hold the long screw in place. The long screw is meant to hold the fixed joints for part B and the forearm part as graphically hinted in Figure 4.1. This long screw is affected by the 140N reaction force of part B from section 4.4.2 and the 138.24N reaction force of the forearm part from section 4.4.1. The two cantilever beams are meant to distribute the shearing stresses caused by the long screw at their joints. The deflection of the upperarm parts can be kept under control by either spacing these components further away from each other or by duplicating and using more of them if necessary. Moreover the weight of the exoskeleton is not taken into consideration which could mean more upperarm parts may be needed. However, optimizing a single upperarm beam and duplicating it is the preferred method to optimize the upper arm part to reduce its material usage.

The upperarm part uses the stress formulas to determine its dimensions but it does not take its deflection into account. This is also true for the optimized upperarm parts calculated in section 4.8.3 of the report.

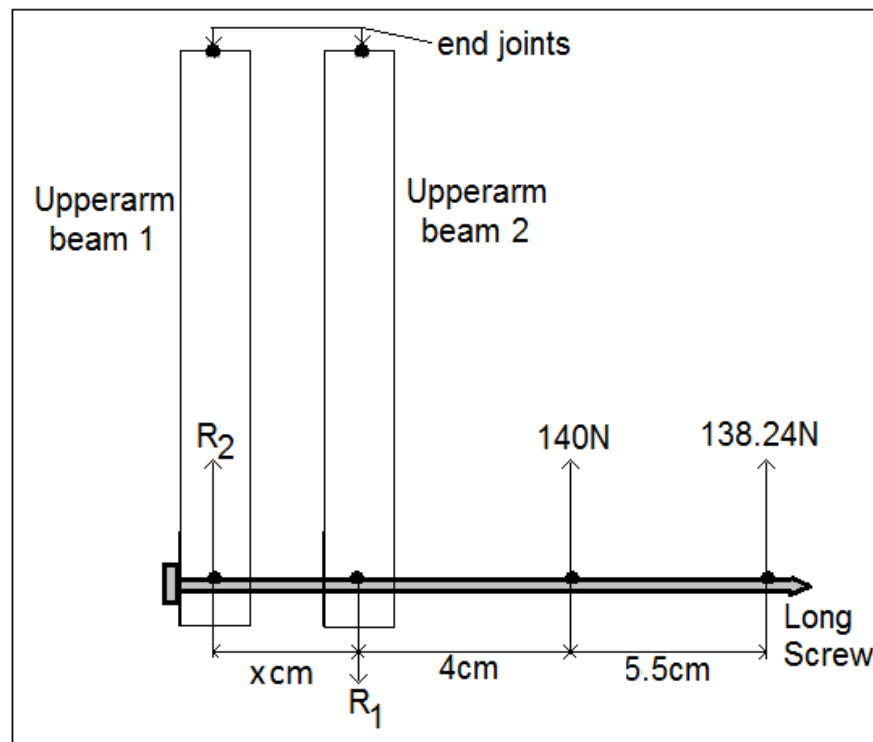


Figure 4.11 Upperarm Diagram

Calculating the reaction forces R_1 and R_2

$$\Sigma M \text{ at } R_2 = 0, -R_1(x) + 140(0.04 + x) + 138.24(0.04 + 0.055 + x) = 0$$

$$R_1 = \frac{18.7328 + 278.24x}{x} = \frac{18.7328}{x} + 278.24$$

Initially the distance between the 140N load and the 138.24N load was 4.5cm while x was set to 3cm and R_1 was calculated to be 861.175N. However this causes a design error where the lowerarm, partB and part F from Figure 4.1 to collide with each other and is undesirable.

To nullify this design error, the distance between the 140N load and the 138.24N load is increase to 5.5cm while the distance ' x ' is adjusted to 3.2cm so that R_1 is near its initial value of 861.175N.

Setting $x=3.2\text{cm}$, R_1 is calculated to be $863.64\text{N} \approx 861.175\text{N}$

$$\Sigma F = 0, R_2 + 140 + 138.24 - 863.64 = 0$$

$$R_2 = 585.4\text{N}$$

$R_1 > R_2$. Thus R_1 is used as the maximum shearing force acting on the upperarm parts.

The Upperarm has a moment load of 125Nm at the end joints and a moment load of 72.5Nm at the joints pierced by the long screw which are both not shown in Figure 4.11. These moments curls into and out of the page.

Calculating the height 'h' for every single upper arm piece needed to withstand the allowable stress of 20MPa using the stress formulas available in section 4.4 of the report.

Case 1: If the shearing stresses causes tensile stresses to the upper arm

Setting $b = 0.02\text{m}$, where $b \neq h$

Total stress of the upperarm;

$$\sigma = \frac{My}{I} = \frac{6M}{bh^2} + \frac{F}{A} = \frac{6(125 + 72.5)}{0.02h^2} + \frac{863.64}{0.02h} = 20\text{MPa}$$

$$h = 0.0555 \approx \mathbf{5.6\text{cm}}$$

Case 2: If the shearing stresses causes bending stresses to the upper arm

Setting $b = 0.02\text{m}$, where $b \neq h$

Total stress of the upperarm;

$$\sigma = \frac{My}{I} = \frac{6M}{bh^2} = \frac{6(125 + 72.5 + 863.64 \times 0.3)}{0.02h^2} = 20\text{MPa}$$

$$h = 0.0828 \approx \mathbf{8.3\text{cm}}$$

Comparing the height 'h' from the calculation results

8.3cm > 5.6cm thus the height 'h' and the width 'b' of the rectangular cross section for every single upper arm piece is design to be 8.3cm and 2cm respectively to ensure that the part at this cross section does not exceed the allowable yield stress.

4.5 FEA results for the exoskeleton parts

This section of the report describes the FEA simulation results obtained from the 3D modelled parts of the exoskeleton.

The methodology of this study is to sketch the proposed exoskeleton before its chosen parts are calculated and modelled in Solidworks, undergoes structural analysis and, is structurally optimized. The optimized parts are then calculated, modelled and, the structural analysis process is repeated for these parts.

The chosen parts of the exoskeleton were initially calculated to have the minimum dimensions needed to either withstand the stress level of 20MPa or to have a maximum deflection of up to 2.5mm. The weight of these parts however was not taken into consideration during the calculation of their dimensions. This could cause the deflections and stresses acting on the exoskeleton parts to be higher than the calculated value. To compensate for this, the maximum allowable yield stress level has been slightly increased to 21MPa while the maximum allowable deflection has increased to 5mm.

Figure 4.12 shows the FEA results for part D. As seen in this figure, the stresses generated upon part D is below the 21MPa range but its deflection is beyond the 5mm. Thus this part is deemed not structurally sound. However this part has been superseded by its optimized version in Figure 4.20. Figure 4.12(a) shows that this part is a simple cantilever beam with a low stress area coloured in blue in the middle. From this figure, Part D can be converted into a truss structure to reduce the blue areas.

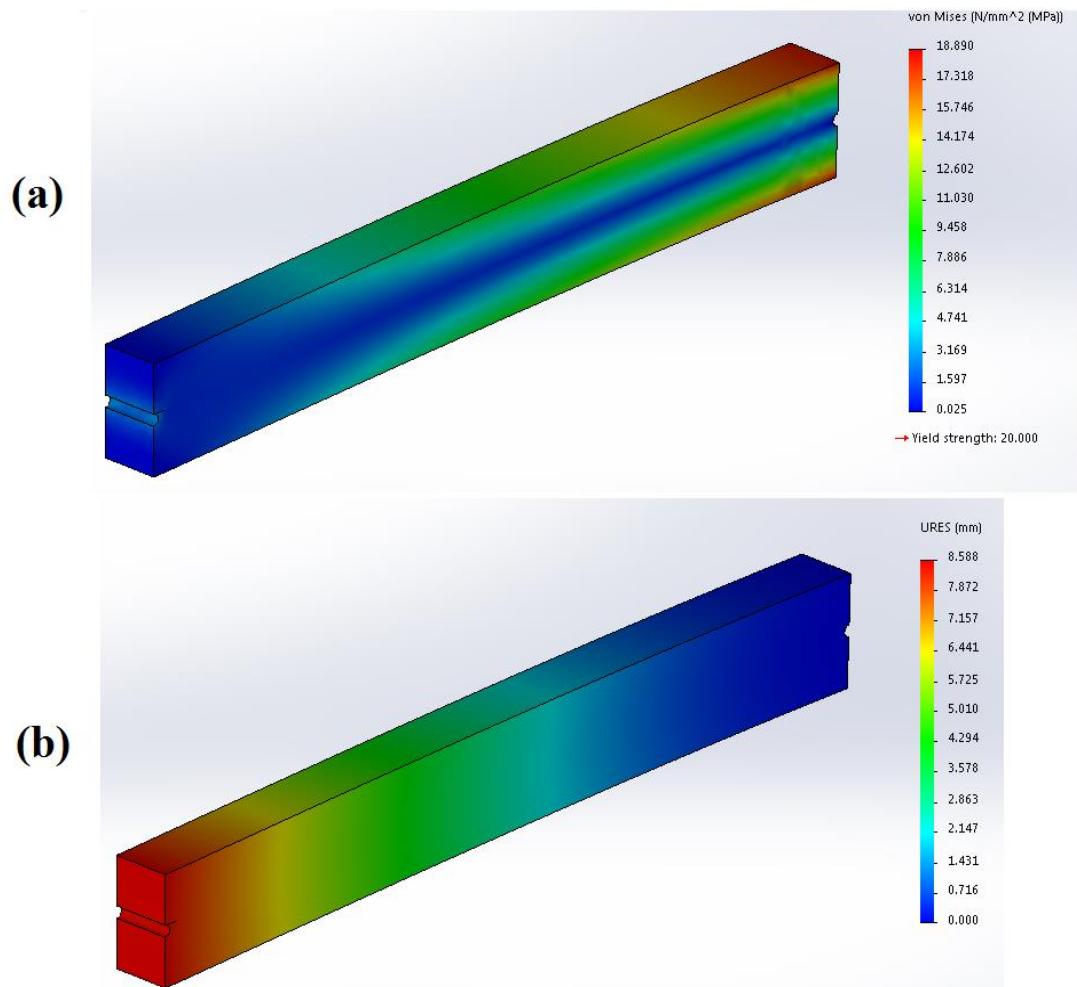


Figure 4.12 Part D FEA results(a) von mises stress results for Part D (b) deflection results for Part D

Figure 4.13 shows the FEA result for Part E. As seen in this figure, the stresses generated upon part E is above the 21MPa and its deflection is beyond the 5mm range. Thus this part has failed but was later superseded by its optimized version in Figure 4.21. The reason for this part to fail may be due to its own weight that is not taken into consideration during calculation that could have resulted in the forces acting on the part to be larger than calculated. Figure 4.13(a) shows that this part is a simple cantilever beam with a low stress area coloured in blue in the middle. From this figure, Part E can be converted into a truss structure to reduce the blue area.

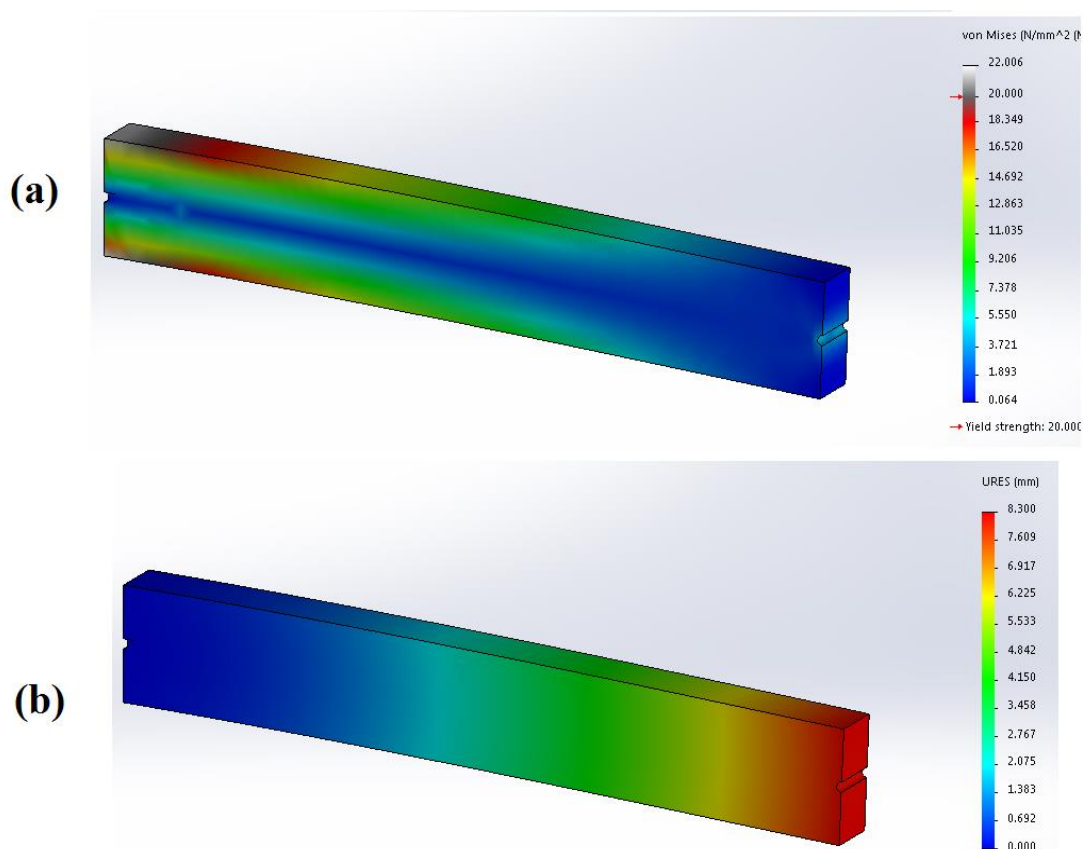
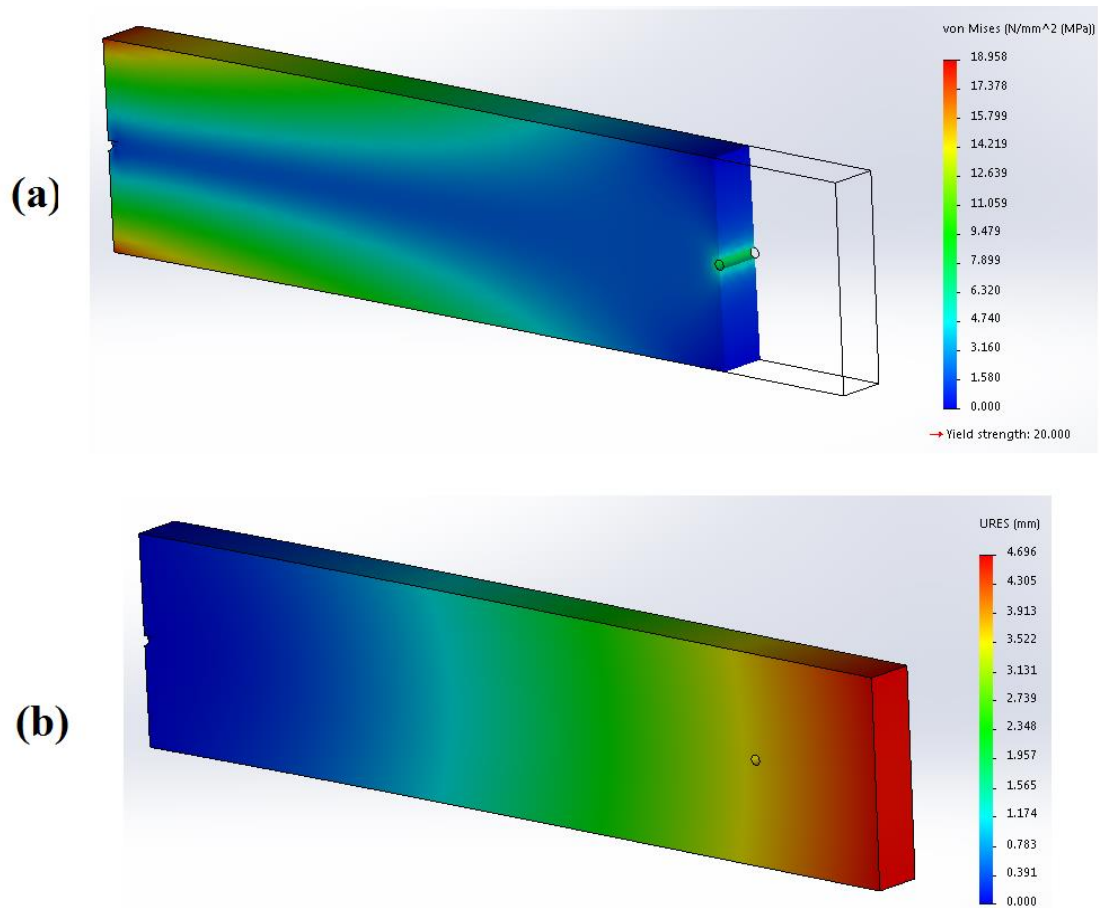


Figure 4.13 Part E FEA results(a) von mises stress results for Part E (b)deflection results for Part E

Figure 4.14 shows the FEA results for the upperarm. As seen in this figure, the stresses generated upon the upperarm are below the 21MPa range and its deflection is below the 5mm range. Thus this part is deemed functional. Figure 4.14(a) shows that this part is a simple cantilever beam with a low stress area coloured in blue in the middle. From this figure, the upperarm part can be converted into a truss structure to reduce the blue area.



**Figure 4.14 Upper Arm FEA results (a) von mises stress results for the upper arm
(b) deflection results for the upper arm**

Figure 4.15 shows the FEA results for part B. As seen in this figure, the stresses generated upon part B are below the 21MPa range and its deflection is below the 5mm range. Thus this part is deemed functional. Figure 4.15(a) shows that this part has the highest stress at the middle section of the L-beam due to torsion and bending. Thus this longer section of the L-beam is replaced with a hollow cylinder.

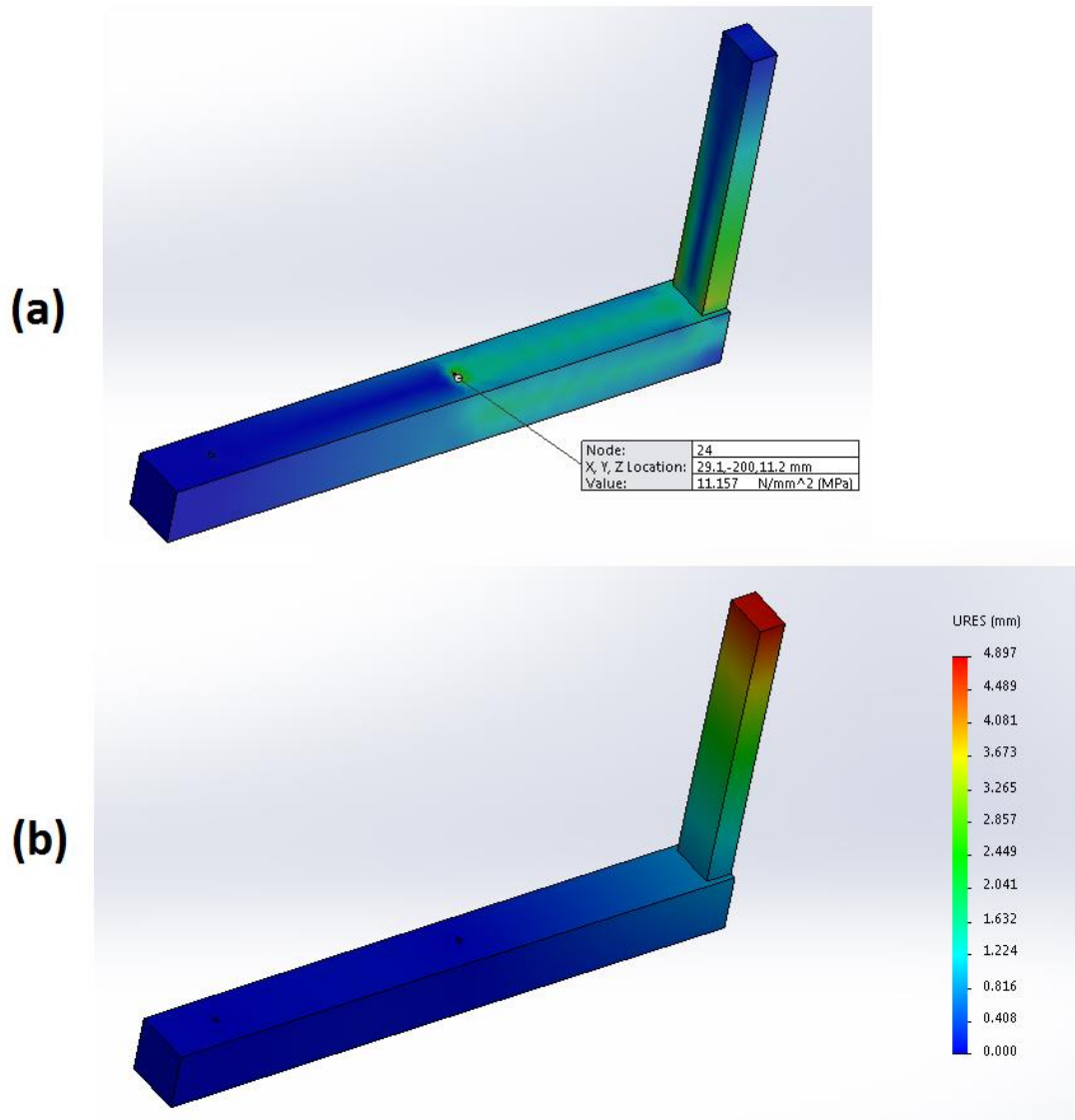


Figure 4.15 Part B FEA results (a) von mises stress results for Part B (b) deflection results for Part B

Figure 4.16 shows the FEA results for the forearm part. As seen in this figure, the stresses generated upon the forearm are below the 21MPa range but its deflection is above the 5mm range. Thus this part is deemed not structurally sound. However this part has been superseded by its optimized version in Figure 4.24. Figure 4.16(a) shows that the part has the highest stress at the middle section of the long beam due to torsion and bending. Thus this beam is replaced with a hollow cylinder.

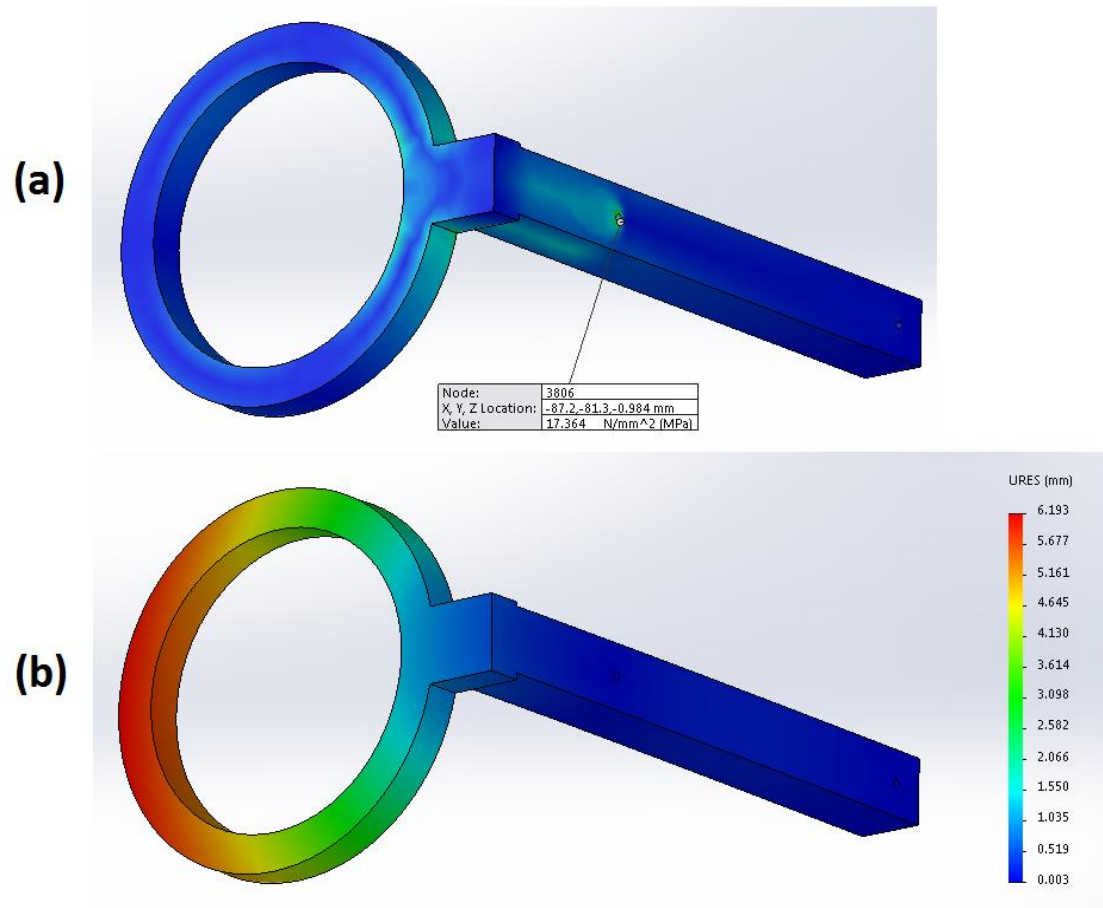


Figure 4.16 lowerarm part FEA results (a) von mises stress results for the lower arm (b) deflection results for the lower arm

4.6 Modelling of the optimized structures

Figure 4.17 shows the truss models for the optimized part D, E and the upper arm. The rest of the other models have simpler structures than the truss structures in Figure 4.17 and are not shown but were revealed in the form of an FEA simulation result presented in section 4.5 and 4.9 of the report.

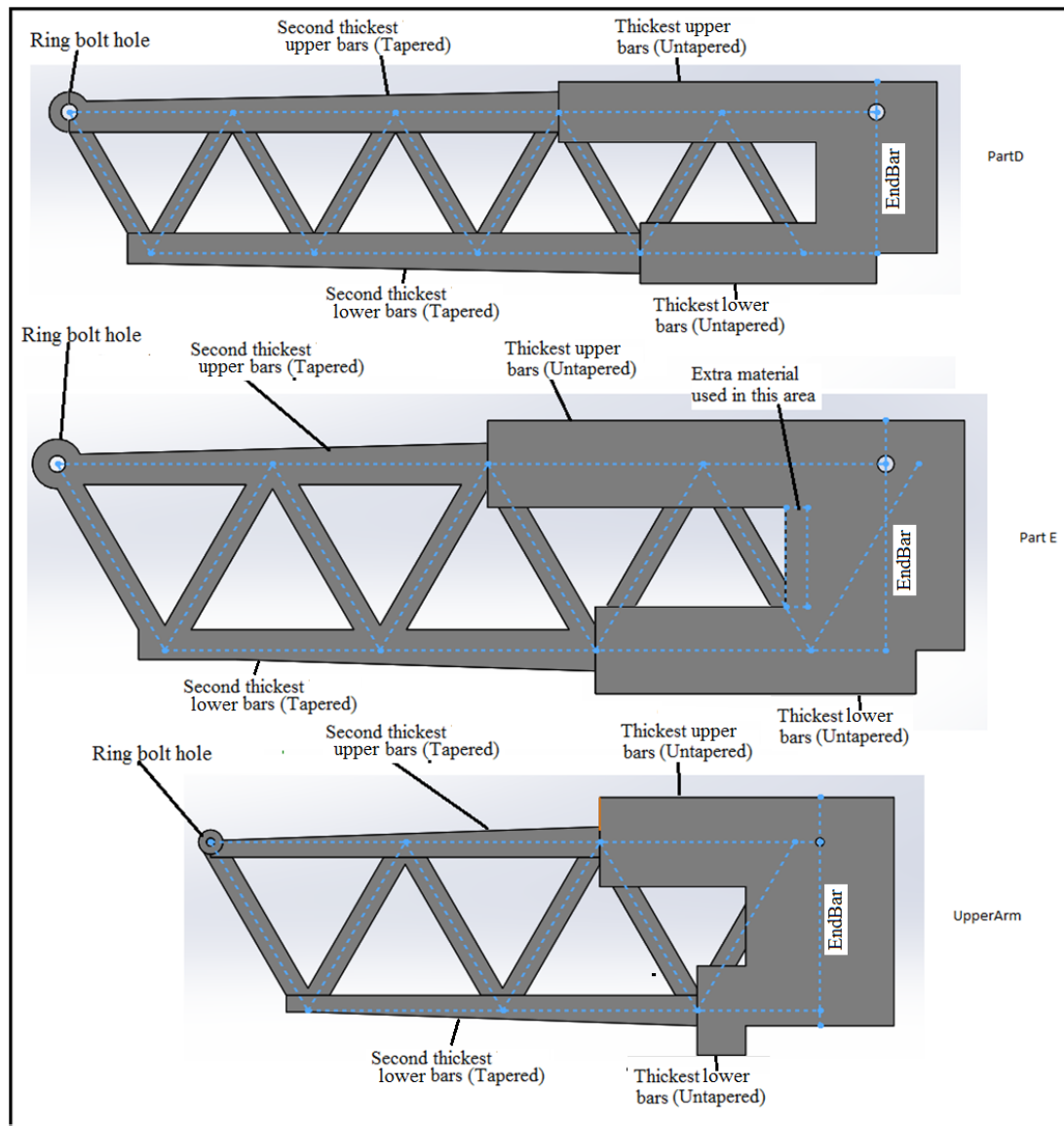


Figure 4.17 Truss Models

4.7 Overview of Calculation for the Optimized PartB and Forearm

Unless specified, the formulas used to calculate the moment of inertia 'I' and the polar moment of inertia 'J' presented in the entire section 4.7 of this report were taken from Ugural (2008). The stress formulas and the deflection formulas from section 4.4 of the report however has been reused in the entire section 4.7 of this report.

The formulas for the moment of inertia 'I' and the polar moment of inertia 'J' for a hollow cylinder according to Ugural (2008) are;

$$J = \frac{\pi}{32} (D^4 - d^4) \quad (16)$$

$$I = \frac{\pi}{64} (D^4 - d^4) \quad (17)$$

Where,

D = Outer Diameter of the hollow cylinder

d = Inner Diameter of the hollow cylinder

As mentioned in section 4.3 of the report, the maximum allowable yield stress and deflections is currently 20MPa and 2.5mm respectively while the young modulus of the material imagined to be used in the parts is 3.5GPa.

In this section of the report, the concept of calculating and producing a pair of results to compare with is similar to Section 4.4 of this report. However, no diagrams were needed as these parts originated from their previously calculated un-optimized parts in Section 4.4 of the report. The inner diameter 'd' and the outer diameter 'D' of a hollow cylinder will be taken as the minimum dimensions required to withstand the allowable stress and deflection limits.

4.7.1 Calculation for the Optimized Forearm Part

The cross section-x of the forearm in Figure 4.6 is a solid square beam of length 28cm and is replaced with a hollow cylinder. The moments and forces acting on this cross section remain the same and that no free body diagram is needed. However, the error of the maximum moment of 96.788Nm from section 4.4.1 is used in the calculations to overdesign its strength. Calculating the dimension of the inner diameter 'd' for the cross section-x of the forearm part needed to withstand the allowable stress of 20MPa using the stress formulas available in section 4.4 of the report.

$$\text{Bending Stress } \sigma = \frac{My}{I} = \frac{(96.766)\left(\frac{D}{2}\right)}{\frac{\pi}{64}(D^4-d^4)} = \frac{985.67D}{(D^4-d^4)}$$

$$\text{Torsional Shear Stress } S = \frac{Tr}{J} = \frac{9.1\left(\frac{D}{2}\right)}{\frac{\pi}{32}(D^4-d^4)} = \frac{46.35D}{(D^4-d^4)}$$

$$\begin{aligned} \text{Maximum principal stress } \sigma_1 &= \frac{\sigma_x + \sigma_y}{2} + \sqrt{\left(\frac{\sigma_x + \sigma_y}{2}\right)^2 + s^2} \\ &= \frac{\frac{985.67D}{(D^4-d^4)} + 0}{2} + \sqrt{\left(\frac{\frac{985.67D}{(D^4-d^4)} + 0}{2}\right)^2 + \frac{46.35D}{(D^4-d^4)}^2} = \frac{987.83D}{(D^4-d^4)} \end{aligned}$$

$$\begin{aligned} \text{Minimum principal stress } \sigma_2 &= \frac{\sigma_x + \sigma_y}{2} - \sqrt{\left(\frac{\sigma_x + \sigma_y}{2}\right)^2 + s^2} \\ &= \frac{\frac{985.67D}{(D^4-d^4)} + 0}{2} - \sqrt{\left(\frac{\frac{985.67D}{(D^4-d^4)} + 0}{2}\right)^2 + \frac{46.35D}{(D^4-d^4)}^2} = \frac{-2.174D}{(D^4-d^4)} \end{aligned}$$

$$\text{The yield stress } \sigma_y = \sqrt{\sigma_1^2 - \sigma_1\sigma_2 + \sigma_2^2}$$

$$= \frac{988.92D}{(D^4-d^4)} = 20MPa$$

For **D= 5.5cm**, d= 5cm

Calculating the dimension of the Outer diameter 'D' for the cross section-x of the fore arm part needed to withstand the allowable Deflection of 2.5mm using the deflection formulas available in Figure 4.5. The deflections are intuitively assumed to be

$$\delta_{total} = \delta_{bending} + \delta_{torsion}$$

$$= \frac{Pb(L^2 - b^2)^{\frac{3}{2}}}{9\sqrt{3}LEI} + \frac{ML^2}{2EI}$$

$$= \frac{(483.83)(0.08)(0.28^2 + 0.08^2)^{\frac{3}{2}}}{9\sqrt{3}(0.28)(E) \times \frac{\pi}{64}(D^4 - d^4)} + \frac{9.1(0.105)^2}{2(E) \times \frac{\pi}{64}(D^4 - d^4)} = 0.0025m$$

If $E = 3.5GPa$ and $d = 5cm$, **$D \approx 5.8cm$**

Comparing the outer diameter 'D' from the calculation results;

5.8cm > 5.5cm thus the outer diameter for the hollow cylinder is taken be 5.8cm and the inner diameter for the hollow cylinder is taken be 5cm. However as mentioned before, the error of the maximum moment value has caused the part to be larger than the intended dimensions but this adds to the structure's strength.

4.7.2 Calculation for the Optimized Part B

The cross section x-x of the Part B in Figure 4.9 is a solid square beam of length 40cm and is replaced with a hollow cylinder. The moments and forces acting on this cross section remains the same and that no free body diagram is needed. However, the error of the maximum moment of 48Nm from section 4.4.2 is used in the calculations to overdesign its strength.

Calculating the dimension of the inner diameter 'd' for the cross section-x of part B needed to withstand the allowable stress of 20MP using the stress formulas available in section 4.4 of the report.

$$\text{Bending Stress } \sigma = \frac{My}{I} = \frac{(48)\left(\frac{D}{2}\right)}{\frac{\pi(D^4-d^4)}{64}} = \frac{1536D}{\pi(D^4-d^4)}$$

$$\text{Torsional Shear Stress } S = \frac{Tr}{J} = \frac{(140)(0.24)\left(\frac{D}{2}\right)}{\frac{\pi(D^4-d^4)}{32}} = \frac{537.6D}{\pi(D^4-d^4)}$$

$$\text{Maximum principal stress } \sigma_1 = \frac{\sigma_x + \sigma_y}{2} + \sqrt{\left(\frac{\sigma_x + \sigma_y}{2}\right)^2 + s^2}$$

$$= \frac{\frac{1536D}{\pi(D^4-d^4)} + 0}{2} + \sqrt{\left(\frac{\frac{1536D}{\pi(D^4-d^4)} + 0}{2}\right)^2 + \left(\frac{537.6D}{\pi(D^4-d^4)}\right)^2} = \frac{542.87D}{(D^4-d^4)}$$

$$\text{Minimum principal stress } \sigma_2 = \frac{\sigma_x + \sigma_y}{2} - \sqrt{\left(\frac{\sigma_x + \sigma_y}{2}\right)^2 + s^2}$$

$$\sigma_2 = \frac{\frac{1536D}{\pi(D^4-d^4)} + 0}{2} - \sqrt{\left(\frac{\frac{1536D}{\pi(D^4-d^4)} + 0}{2}\right)^2 + \left(\frac{537.6D}{\pi(D^4-d^4)}\right)^2} = \frac{-53.94D}{(D^4-d^4)}$$

The yield stress $\sigma_y = \sqrt{\sigma_1^2 - \sigma_1\sigma_2 + \sigma_2^2}$

$$= \frac{571.75D}{(D^4 - d^4)} = 20MPa$$

For $D= 6.9\text{cm}$, $d=0.0689 \approx 6.9\text{cm}$

Calculating the dimension of the Outer diameter 'D' for the cross section-x of the fore arm part needed to withstand the allowable Deflection of 2.5mm using the deflection formulas available in Figure 4.5. The deflections are intuitively assumed to be

$$\delta_{total} = \delta_{bending} + \delta_{torsion}$$

$$= \frac{WL^3}{48EI} + \frac{FL^3}{2EI}$$

$$= \frac{(280)(0.2)^3}{48(E) \times \frac{\pi}{64} (D^4 - d^4)} + \frac{140(0.24)^3}{2(E) \times \frac{\pi}{64} (D^4 - d^4)} = 0.0025 \text{ m}$$

For $E = 3.5GPa$ and $D = 6.9\text{cm}$,

$$d = 0.0671 \approx 6.7 \text{ cm}$$

Comparing the inner diameters of the results;

6.7cm < 6.9cm. Thus the outer diameter for the hollow cylinder is taken be 6.9cm and the inner diameter for the hollow cylinder is taken be 6.7cm. However, the new deflection value due to reasons stated in section 4.9 of the report is 5mm. During the FEA simulation of this part, its deflection value have reached beyond the 5mm mark and is undesirable. To make the deflection of this part slightly lesser but near to the un-optimized part B's deflection result shown in Figure 4.15 (b) while maintaining its value to be below the 5mm mark, the inner diameter of the optimized part B's hollow cylinder was set to a new value of 6.2cm. The optimized part B's inner

diameter's dimension with a value of 6.2cm originates from the FEA simulation processes and not by calculation. However this makes the fore mentioned part larger than calculated resulting in this part being stronger than intended. The total mass of this part however remains lower than its un-optimized counterpart even with the newly amended inner diameter's dimension of 6.2cm and is shown in Table 2

4.8 Overview Calculation for the Optimized Part D, E and the upperarm

Unless specified, the moment of inertia 'I' formula, the polar moment of inertia 'J' formula, the stress formulas and the deflection formulas from section 4.4 of the report has been reused in the entire section 4.8 of this report.

As mentioned in section 4.3 of the report, the maximum allowable yield stress and deflections is currently 20MPa and 2.5mm respectively while the young modulus of the material imagined to be used in the parts is 3.5GPa.

The Part D, E and the upper arm from Figure 4.1 are simple cantilever beams and are replaced with trusses. The development of the truss structure template shown in Figure 4.18 (a) and the method to calculate its forces were taken and learnt from Lovett's (2013) tutorials. The cross sections for all of the bars used in the truss template were taken to be either a rectangular or a square cross section. The tapering plan shown in Figure 4.18 (b) however was intuitively derived from this truss template developed from Lovett's (2013) tutorials. The truss template and the tapering plans are used in the development of the optimized Part D, E and the upperarm.

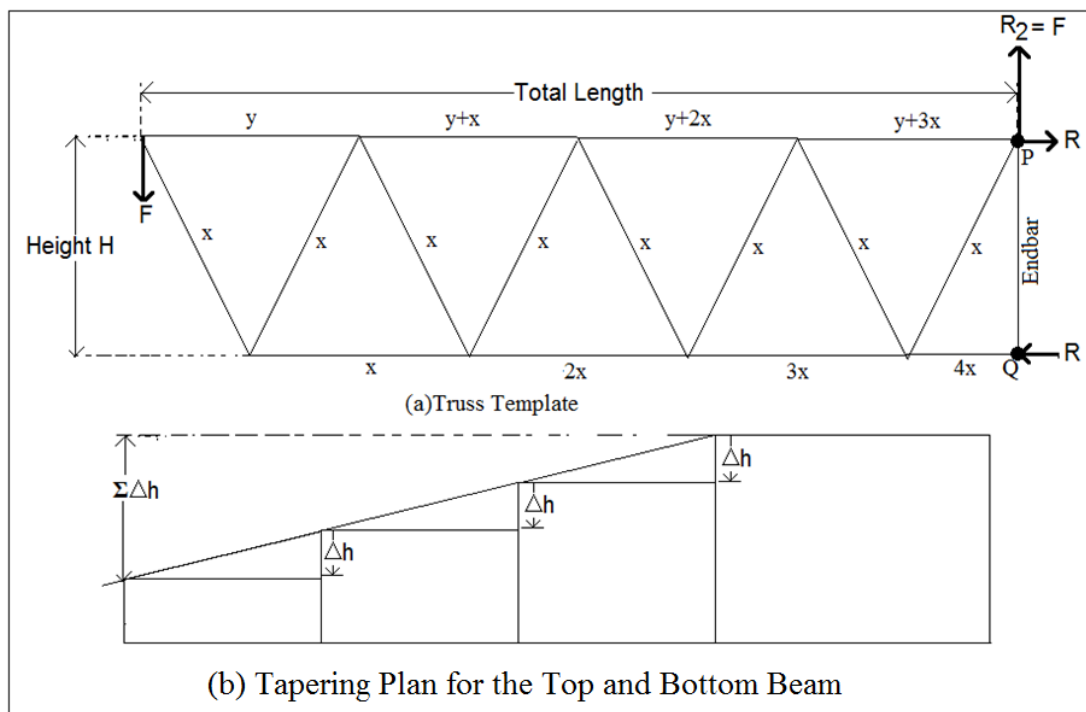


Figure 4.18 Truss template developed from Lovett's (2013) tutorials and the intuitively calculated tapering plan.

Based on Lovett's (2013) tutorials the forces 'x' and 'y' from Figure 4.18(a) were intuitively calculated to be;

$$x = \frac{F}{\sin 60} \quad (18)$$

$$y = \frac{F}{\tan 60} \quad (19)$$

Where,

x = force, N

y = force, N

F = force, N

Bar PQ that is also labelled as the EndBar acts as a base for the truss template structure.

To begin developing the truss structures used to optimize the part D, E and the upperarm, The truss height H in Figure 4.18(a) is first defined and the individual bar lengths of the truss structure is calculated using simple trigonometry as;

$$\text{barlength} = \frac{H}{\sin 60} \quad (20)$$

Where

H=truss height, m

barlength = individual bar lengths of the truss structure, m

The total number of upper bars is calculated as;

$$\text{Total number of upper bars} = \frac{\text{Total Length}}{\text{barlength}} \quad (21)$$

Where,

Total length= total length of the truss structure, m

barlength = individual bar lengths of the truss structure, m

The reaction force R in Figure 4.18(a) is calculated using

$$R = \frac{F(\text{Total Length})}{H} \quad (22)$$

Where,

F=Force, m

H= truss height, m

Total length= total length of the truss structure, m

The EndBar is a rectangular bar that undergoes bending stress due to R. Using the stress formulas in section 4.4 of the report, the total stress of this bar is;

$$\text{stress } \sigma = \frac{My}{I} \quad (23)$$

where

M=moment, Nm

$$y = \frac{\text{height of bar}}{2}, \text{m}$$

I = moment of inertia, m^4

This stress formula will be used to determine the minimum dimensions for the EndBar's rectangular cross section. The middle bars subjected to the force 'x' as shown in Figure 4.18(a) are calculated as follows;

$$\text{Force on middle bar} = x = \frac{\text{Force}}{\sin 60} \quad (24)$$

These middle bars have a square cross section and are assumed to undergo tension/compression stresses. Reusing the tensile/compression stress formula from section 4.4 of the report, the minimum dimensions of the cross sections needed to withstand the allowable yield stress 20MPa is calculated as;

$$\text{Middle Bar tensile/compression stress} = \frac{F}{A} \quad (25)$$

Where,

F= force, N

A=area, m^2

The top bar connected to point Q only has a tensile stress due to R. the effect from the force R causes the upper bar at point Q to have the second largest dimension of the truss structure. Reusing the tensile/compression stress formula from section 4.4 of the report, the stress acting on this bar is;

$$\text{stress} = \frac{\text{Force}}{\text{Area}} \quad (26)$$

This fore mentioned bar is the second thickest upper or lower beam of the truss models shown in Figure 4.17. The fore mentioned stress formula will be used to determine the minimum dimension for the second thickest upper or lower beams.

The top bar connected to point P has a bending stress due to R2 and a tensile stress due to R. The effect from these forces R2 and R causes the upper bar at point P to have the largest dimension of the truss structure. Using the stress formulas in section 4.4 of the report, the total stress of this bar is,

$$\text{Total stress} = \frac{F}{A} + \frac{My}{I} \quad (27)$$

Where

F= Force, N

A= area, m^2

M= moment, Nm

$y = \frac{\text{height of bar}}{2}$, m

I= moment of inertia, m^4

This fore mentioned bar is also the thickest upper or lower beam of the truss models shown in Figure 4.17. The fore mentioned stress formula will be used to determine the minimum dimension for the thickest upper or lower beams.

To intuitively develop the taper bar plan in Figure 4.18 (b), each upper and lower beam is assumed to undergo tensile stress. Reusing the tensile/compression stress formula from section 4.4 of the report, the stress of these bars is calculated as

$$stress = \frac{F}{A} = \frac{F}{b \times height} \quad (28)$$

$$Height = \frac{F}{b\sigma} \quad (29)$$

Where,

F= force, m

A= Area, m^2

σ = stress, Pa

h= height, m

b=width, m

This formula shows the minimal dimension of the height ‘h’ needed by each top and bottom beam to not exceed the maximum allowable yield stress. The difference between each corresponding beam’s height is used to create a triangular tapering structure for the top and bottom beams shown in Figure 4.18 (b). This consequently increases the material usage of the entire structure slightly but it simplifies the design for manufacturing ease. From Figure 4.18 (b), the height difference Δh between 2 bars

$$\Delta h = h - h_o = \frac{F - F_o}{b\sigma} \quad (30)$$

Where,

Δh = height difference, m

b=width, m

σ =stress, Pa

h = height of the 1st bar, m

h_o = height of the 2nd bar, m

F = force for the 1st bar, N

F_o = force for the 2nd bar, N

referring to the first 2 upper bars near the force F in Figure 4.18(a), $F =$
force for the 1st bar = y + x and, $F_o =$ *force for the 2nd bar = y*

$$F - F_o = x = \frac{F}{\sin 60} \quad (31)$$

$$\text{Thus } \Delta h = \frac{F - F_o}{b\sigma} = \frac{F}{\sin 60 b\sigma} \quad (32)$$

$$\Sigma \Delta h = \text{Total number of upper or lower beams} \times \Delta h \quad (33)$$

Where,

$F =$ *force for the 1st bar, N*

$F_o =$ *force for the 2nd bar, N*

$x =$ *force, N*

$F =$ *force, N*

$b =$ *width, m*

$\sigma =$ *stress, Pa*

$\Delta h =$ *height difference, m*

$\Sigma \Delta h =$ *total height difference, m*

The total height difference $\Sigma \Delta h$ can be used to determine the taper dimensions of the upper and lower bar. If the total number of upper beams does not equal the total number of lower beams then the $\Sigma \Delta h$ dimension will have to be calculated and used separately for the top and bottom beam sections. Thus the tapering plan has been intuitively developed.

Referring to the truss models in Figure 4.17, the ring bolt holes modeled at the tip of these truss structures is assumed to be 2 rectangular cantilever beams as illustrated in Figure 4.19.

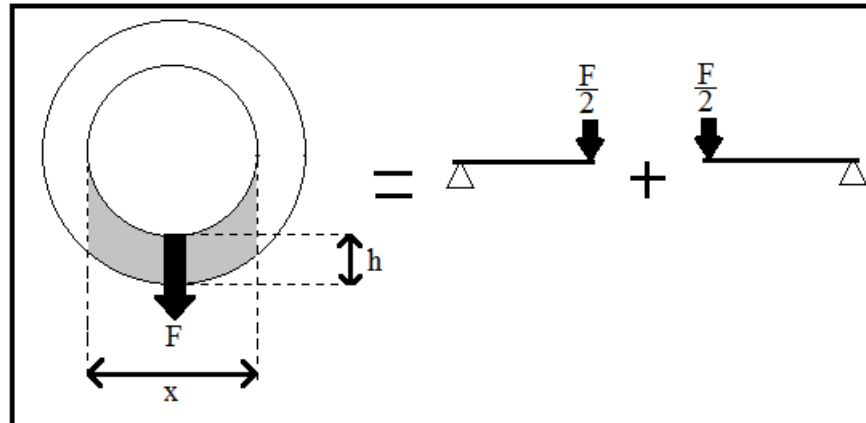


Figure 4.19 Ring Bolt Hole Plan

The bending stress formula for a cantilever beam (Ugural, 2008) is given as;

$$\sigma = \frac{My}{I} \quad (34)$$

where,

$$M = \frac{F}{2} \times \frac{x}{2}, \text{ Nm}$$

F= Force, N

x = the bolt diameter, m

I=moment of inertia, mm^2

This formula will be used to determine the minimum thickness 'h' of the ring bolt hole. The bolt diameter x is currently set to 0.004m.

The calculations for the optimized part D, E and the upperarm are based upon Figure 4.18, Figure 4.19 and the solidworks 3D truss models in Figure 4.17.

4.8.1 Calculation for the Optimized Part D

Using the truss template in Figure 4.18, the beam height of the un-optimized part is calculated and chosen to be 3.7cm.

Thus the truss height $H = 3.7\text{cm}$

$$\text{barlength} = \frac{H}{\sin 60} = \frac{3.7}{\sin 60} \approx 4.3\text{cm}$$

$$\text{Total number of upper bars} = \frac{\text{Total length}}{\text{barlength}} = \frac{0.2}{0.0427} = 4.68 \approx 4.5 \text{ bars}$$

This number of upper bars may decrease if the end bar that supports the reaction loads becomes too thick

The force acting on the truss structure $F = 280\text{N}$

$$\text{Reaction Force } R = \frac{F(\text{Total length})}{H} = \frac{(280)(0.2)}{0.035} = 1600\text{N}$$

Setting $b = 0.02\text{m}$,

Reusing the bending stress formula from section 4.4 of the report, the End Bar bending stress is calculated as;

$$\sigma = \frac{My}{I} = \frac{6M}{bh^2} = \frac{6(1600 \times 0.037)}{0.02h^2} = 20\text{MPa}$$

$$h = 0.0297 \approx 3\text{cm}$$

Thus the minimum dimensions of the rectangular cross sectional area of the EndBar needed to withstand the allowable yield stress is taken as $2 \times 3 \text{ cm}^2$

Setting $b = h$,

$$\text{Force on Middle bar} = \frac{F}{\sin 60} = \frac{280}{\sin 60} = 323.316N$$

Reusing the tensile/compression stress formula from section 4.4 of the report, the middle bar tensile stress is calculated as;

$$\sigma = \frac{F}{h^2} = \frac{323.316}{h^2} = 20MPa$$

$$h = 0.0037 \approx 4mm$$

Thus the minimum dimensions of the square cross sectional area of the middle bar needed to withstand the allowable yield stress is taken as $4 \times 4 \text{ mm}^2$. During simulation however, these bars are made to have a rectangular cross section of $b = 6mm$ and $h = 5mm$. The explanation for this increase in dimension is covered in section 4.9 of the report.

Setting $b = h$,

Reusing the tensile/compression stress formula from section 4.4 of the report, the stress for the second thickest upper and lower bar is calculated as;

$$\sigma = \frac{F}{h^2} = \frac{1600}{h^2} = 20MPa$$

$$h = 0.089 \approx 9mm$$

Thus the minimum dimensions of the square cross sectional area for the second thickest upper and lower bars shown in Figure 4.17 needed to withstand the allowable yield stress is taken as $9 \times 9 \text{ mm}^2$. During simulation however, these bars are made to be $b = 1cm$, $h = 1cm$. The explanation for this increase in dimension is covered in section 4.9 of the report.

Setting $b = 0.02\text{m}$,

Reusing the stress formulas from section 4.4 of the report, the stress for the thickest upper and lower bar is calculated as;

$$\sigma = \frac{F}{A} + \frac{My}{I} = \frac{F}{bh} + \frac{6M}{bh^2} = \frac{1600}{h^2} + \frac{6(280)(0.035)}{0.02h^2} = 20\text{MPa}$$

$$h = 0.0143 \approx 1.5\text{cm}$$

Thus the minimum dimensions of the rectangular cross sectional area for the thickest upper and lower bars shown in Figure 4.17 needed to withstand the allowable yield stress is taken as $2 \times 1.5\text{cm}^2$.

Tapering for the second thickest upper and lower beams

$$\Delta h = \frac{F}{\sigma b \sin 60} = \frac{280}{\sin 60 (0.02) (20\text{MPa})} = 0.00081 \approx 8.1\text{mm}$$

Referring to Figure 4.17, the total number of the second thickest upper or lower beams is 3.

$$\begin{aligned} \Sigma \Delta h &= \text{Total number of upper or lower beams} \times \Delta h \\ &= 3 \times 8.1\text{mm} = 24.3\text{mm} \end{aligned}$$

Thus the total height difference $\Sigma \Delta h$ used to taper the second thickest upper and lower beams is 24.3mm

Calculating the ring bolt hole's thickness 'h' for Part D in Figure 4.17

Setting $b = 0.02\text{m}$,

Reusing the bending stress formula from section 4.8 of the report, the stress for the ring bolt hole is assumed to be;

$$\sigma = \frac{My}{I} = \frac{6\left(\frac{F}{2} \times \frac{x}{2}\right)}{bh^2} = \frac{6\left(\frac{280}{2} \times \frac{0.004}{2}\right)}{0.02h^2} = 20\text{MPa}$$

$$h = 0.00205 \approx 2\text{mm}$$

Thus the minimum thickness 'h' of the ring bolt hole assumed to be able to withstand the allowable yield stress is 2mm

4.8.2 Calculation for the Optimized Part E

Using the truss template in Figure 4.18, the beam height of the un-optimized part is calculated and chosen to be 4.5cm.

Thus the truss height $H = 4.5\text{cm}$

$$\text{barlength} = \frac{H}{\sin 60} = \frac{4.5}{\sin 60} \approx 5.2\text{cm}$$

$$\text{Total number of upper bars} = \frac{\text{Total length}}{\text{barlength}} = \frac{0.2}{0.052} = 4 \approx 4\text{bars}$$

The number of upper bars may decrease if the end bar that supports the reaction loads becomes too thick

The force acting on the truss structure $F = 483.83N$

$$\text{Reaction Force } R = \frac{F(\text{Total length})}{H} = \frac{(483.83)(0.2)}{0.045} = 2150.37N$$

Setting $b = 0.02m$,

Reusing the bending stress formula from section 4.4 of the report, the End Bar bending stress is calculated as;

$$\sigma = \frac{My}{I} = \frac{6M}{bh^2} = \frac{6(2150.37 \times 0.045)}{0.02h^2} = 20MPa$$

$$h = 0.038 \approx 3.8cm$$

Thus the minimum dimensions of the rectangular cross sectional area of the EndBar needed to withstand the allowable yield stress is taken as $2 \times 3.8 \text{ cm}^2$

setting $b = h$,

$$\text{Force on Middle bar} = \frac{483.83}{\sin 60} = 558.68N$$

Reusing the tensile/compression stress formula from section 4.4 of the report, the middle bar tensile stress is calculated as;

$$\sigma = \frac{F}{h^2} = \frac{558.68}{h^2} = 20MPa$$

$$h = 0.00528 \approx 6mm$$

Thus the minimum dimensions of the square cross sectional area of the middle bar needed to withstand the allowable yield stress is taken as $6 \times 6 \text{ mm}^2$. During simulation however, these bars are made to have a rectangular cross section of $b = 1.1mm$ and $h = 6mm$. The explanation for this increase in dimension is covered in section 4.9 of the report.

setting $b = h$,

Reusing the tensile/compression stress formula from section 4.4 of the report, the stress for the second thickest upper and lower bar is calculated as;

$$\sigma = \frac{F}{h^2} = \frac{2150.37}{h^2} = 20MPa$$

$$h = 0.0104 \approx 1cm$$

Thus the minimum dimensions of the square cross sectional area for the second thickest upper and lower bars shown in Figure 4.17 needed to withstand the allowable yield stress is taken as $1 \times 1 \text{ cm}^2$. During simulation however, these bars are made to be $b=1.1cm$, $h=1.1cm$. The explanation for this increase in dimension is covered in section 4.9 of the report.

Setting $b = 0.02m$,

Reusing the stress formulas from section 4.4 of the report, the stress for the thickest upper and lower bar is calculated as;

$$\sigma = \frac{F}{A} + \frac{My}{I} = \frac{F}{bh} + \frac{6M}{bh^2} = \frac{2150.37}{h^2} + \frac{6(483.83)(0.045)}{0.02h^2} = 20MPa$$

$$h = 0.0209 \approx 2.1cm$$

Thus the minimum dimensions of the rectangular cross sectional area for the thickest upper and lower bars shown in Figure 4.17 needed to withstand the allowable yield stress is taken as $2 \times 2.1 \text{ cm}^2$.

Tapering for the second thickest upper and lower beams

$$\Delta h = \frac{F}{\sigma b \sin 60} = \frac{483.83}{\sin 60 (0.02)(20 \text{MPa})} = 0.00139 \approx 1.4 \text{mm}$$

Referring to Figure 4.17, the total number of the second thickest upper or lower beams is 2.

$$\begin{aligned} \Sigma \Delta h &= \text{Total number of upper or lower beams} \times \Delta h \\ &= 2 \times 1.4 \text{mm} = 2.8 \text{mm} \end{aligned}$$

Thus the total height difference $\Sigma \Delta h$ used to taper the second thickest upper and lower beams is 2.8mm

Calculating the ring bolt hole's thickness 'h' for Part E in Figure 4.17

Setting $b = 0.02\text{m}$,

Reusing the bending stress formula from section 4.8 of the report, the stress for the ring bolt hole is assumed to be;

$$\sigma = \frac{My}{I} = \frac{6\left(\frac{F}{2} \times \frac{x}{2}\right)}{bh^2} = \frac{6\left(\frac{483.83}{2} \times \frac{0.004}{2}\right)}{0.02h^2} = 20 \text{MPa}$$

$$h = 0.00269 \approx 2 \text{mm}$$

Thus the minimum thickness 'h' of the ring bolt hole assumed to be able to withstand the allowable yield stress is 2mm

4.8.3 Calculation for the Optimized Upper arm

Using the truss template in Figure 4.18, the beam height of the un-optimized part is calculated and chosen to be 4.5cm.

Thus the truss height $H = 8.3\text{cm}$

$$\text{barlength} = \frac{H}{\sin 60} = \frac{8.3}{\sin 60} \approx 9.6\text{cm}$$

$$\text{Total number of upper bars} = \frac{\text{Total length}}{\text{barlength}} = \frac{0.3}{0.096} = 3.13 \approx 3\text{bars}$$

The number of upper bars may decrease if the end bar that supports the reaction loads becomes too thick

The force acting on the truss structure $F = \frac{125+72.5}{0.3} \times \frac{1}{2} + 861.175 = 1189.76\text{N}$

$$\text{Reaction Force } R = \frac{F(\text{Total length})}{H} = \frac{(1189.76)(0.3)}{0.083} = 4302.44\text{N}$$

Setting $b = 0.02\text{m}$,

Reusing the bending stress formula from section 4.4 of the report, the End Bar bending stress is calculated as;

$$\sigma = \frac{My}{I} = \frac{6M}{bh^2} = \frac{6(4302.44 \times 0.083)}{0.02h^2} = 20\text{MPa}$$

$$h = 0.073 \approx 7.3\text{cm}$$

Thus the minimum dimensions of the rectangular cross sectional area of the EndBar needed to withstand the allowable yield stress is taken as $2 \times 7.3 \text{ cm}^2$

Setting $b = h$,

$$\text{Force on Middle bar} = \frac{1189.76}{\sin 60} = 1373.82N$$

Reusing the tensile/compression stress formula from section 4.4 of the report, the middle bar tensile stress is calculated as;

$$\sigma = \frac{F}{h^2} = \frac{1373.82}{h^2} = 20MPa$$

$$h = 0.00829 \approx 8.3\text{mm}$$

Thus the minimum dimensions of the square cross sectional area of the middle bar needed to withstand the allowable yield stress are taken as $9 \times 9\text{mm}^2$.

Setting $b = h$,

Reusing the tensile/compression stress formula from section 4.4 of the report, the stress for the second thickest upper and lower bar is calculated as;

$$\sigma = \frac{F}{h^2} = \frac{4302.44}{h^2} = 20MPa$$

$$h = 0.0147 \approx 1.5\text{cm}$$

Thus the minimum dimensions of the square cross sectional area for the second thickest upper and lower bars shown in Figure 4.17 needed to withstand the allowable yield stress is taken as $1.5 \times 1.5\text{cm}^2$.

Setting $b = 0.02\text{m}$,

Reusing the stress formulas from section 4.4 of the report, the stress for the thickest upper and lower bar is calculated as;

$$\sigma = \frac{F}{A} + \frac{My}{I} = \frac{F}{bh} + \frac{6M}{bh^2} = \frac{4302.44}{0.02h} + \frac{6(1373.82)(0.083)}{0.02h^2} = 20\text{MPa}$$

$$h = 0.0442 \approx 4.4\text{cm}$$

Thus the minimum dimensions of the rectangular cross sectional area for the thickest upper and lower bars shown in Figure 4.17 needed to withstand the allowable yield stress is taken as $2 \times 4.4\text{cm}^2$.

Tapering for the second thickest upper and lower beams

$$\Delta h = \frac{(1189.76)}{\sin 60(0.02)(20\text{MPa})} = 0.00344 \approx 3.4\text{mm}$$

Referring to Figure 4.17, the total number of the second thickest upper or lower beams is 2.

$$\Sigma \Delta h = \text{Total number of upper or lower beams} \times \Delta h$$

$$= 2 \times 3.4\text{mm} = 6.8\text{mm}$$

Thus the total height difference $\Sigma \Delta h$ used to taper the second thickest upper and lower beams is 6.8mm

Calculating the ring bolt hole's thickness 'h' for the upperarm in Figure 4.17

Setting $b = 0.02\text{m}$,

Reusing the bending stress formula from section 4.8 of the report, the stress for the ring bolt hole is assumed to be;

$$\sigma = \frac{My}{I} = \frac{6\left(\frac{F}{2} \times \frac{x}{2}\right)}{bh^2} = \frac{6\left(\frac{1189.76}{2} \times \frac{0.004}{2}\right)}{0.02h^2} = 20\text{MPa}$$

$$h = 0.00422 \approx 4\text{mm}$$

Thus the minimum thickness 'h' of the ring bolt hole assumed to be able to withstand the allowable yield stress is 4mm

4.9 FEA results for the optimized exoskeleton parts.

This section of the report describes the FEA simulation results obtained from the optimized 3D modelled parts of the exoskeleton. From these results, the effects or changes that arise due to the design optimization of the parts is reported in this section of the report.

The methodology of this study is to sketch the proposed exoskeleton before its chosen parts are calculated and modelled in Solidworks, undergoes structural analysis and, is structurally optimized. The optimized parts are then calculated, modelled and, the structural analysis process is repeated for these parts.

The optimized parts of the exoskeleton were initially calculated to have the minimum dimensions needed to either withstand the stress level of 20MPa or to have a maximum deflection of up to 2.5mm. The weight of these parts however was not taken into consideration during the calculation of their dimensions. This could cause the deflections and stresses acting on the exoskeleton parts to be higher than the

calculated value. To compensate for this, the maximum allowable yield stress level has been slightly increased to 21MPa while the maximum allowable deflection has increased to 5mm.

The dimensions of some of the truss bars of the optimized part D, E and the upperarm shown in Figure 4.20, Figure 4.21 and, Figure 4.22 respectively are made to be slightly thicker than the intended calculated value because the stresses caused by the structure's own weight during simulation cause the stress acting on these beams to be higher than calculated.

Figure 4.20 shows the FEA results for the optimized part D. As seen in this figure, the stresses generated upon the optimized part D is below the 21MPa range and its deflection is also below the 5mm. Thus the part is deemed functional.

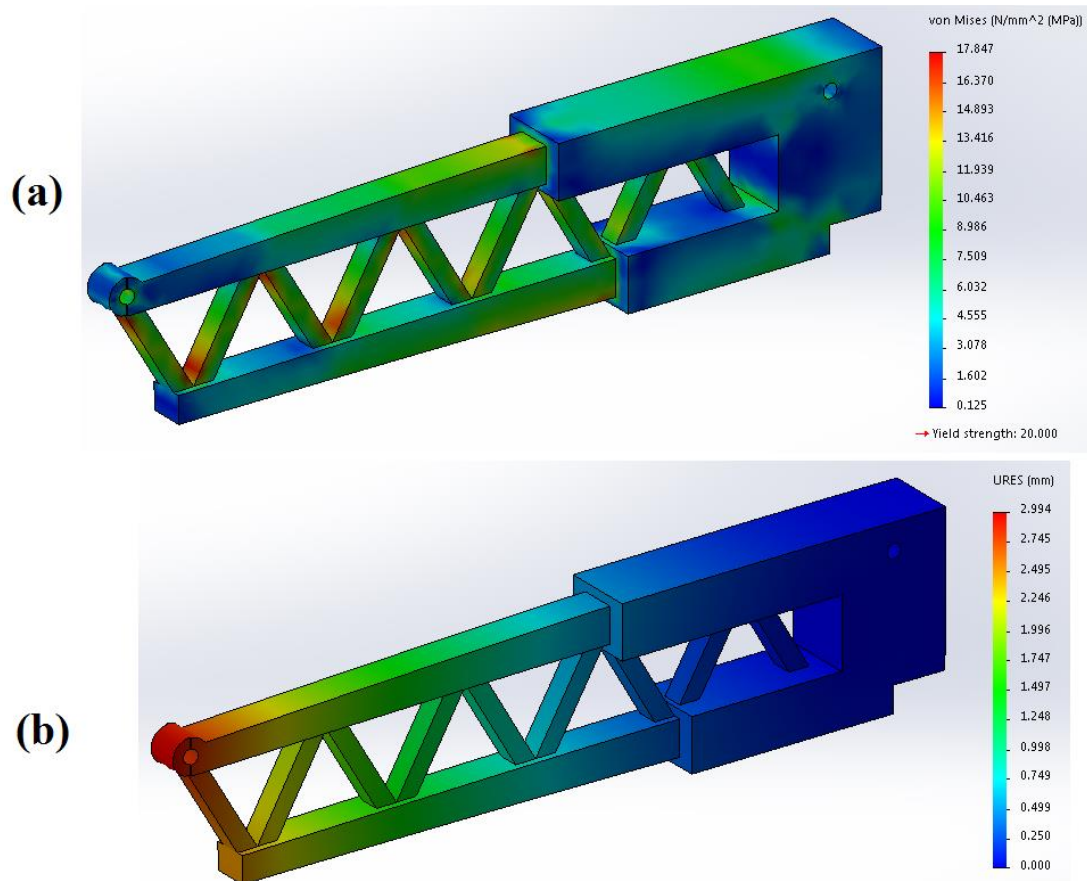


Figure 4.20 Optimized Part D FEA results (a) von mises stress results for the optimized Part D (b) deflection results for the optimized Part D

Figure 4.21 shows the FEA results for the optimized part E. As seen in this figure, the stresses generated upon the optimized part E is below the 21MPa range and its deflection is also below the 5mm. Thus the part is deemed functional. Of all the FEA results presented in this report, this part is the only part that has a deflection lower than 2.5mm.

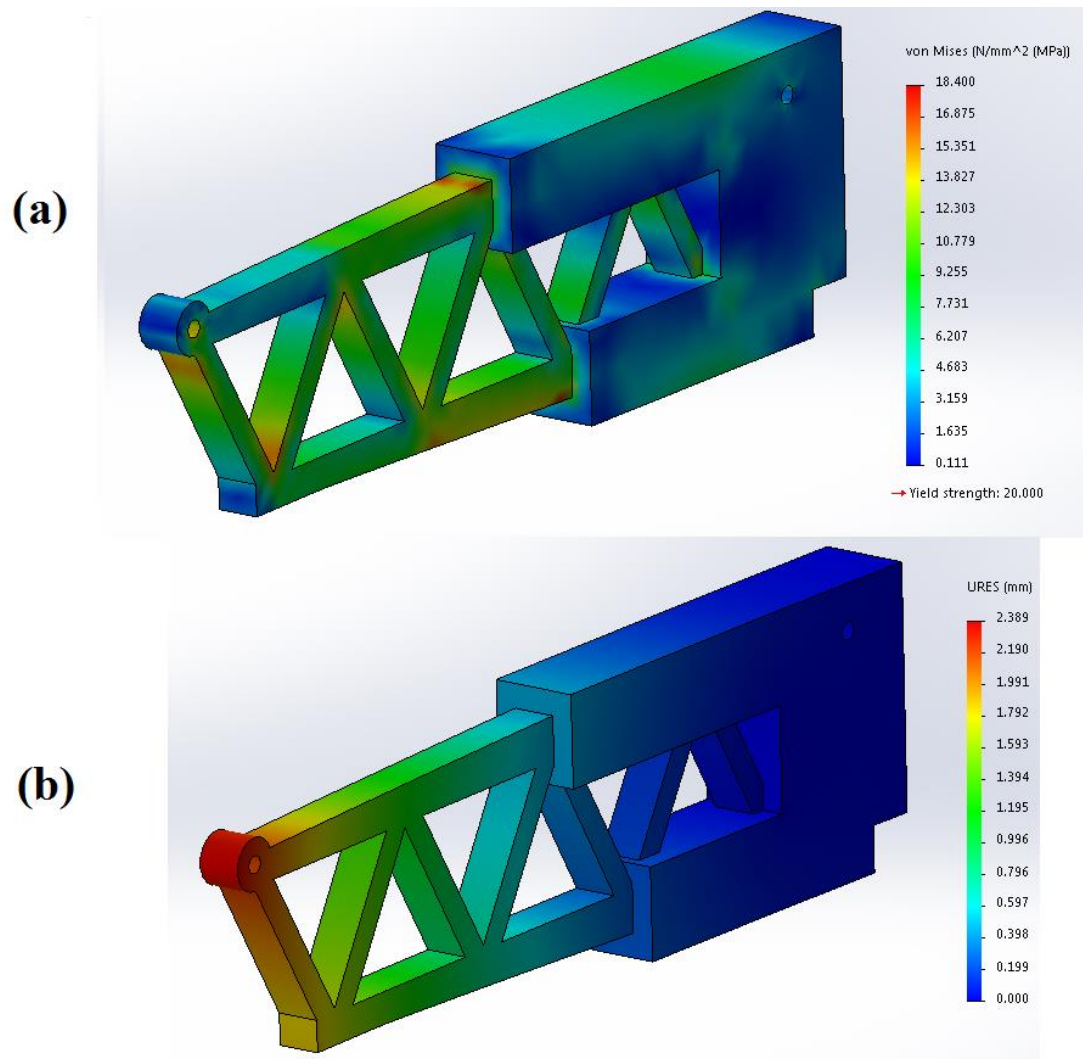


Figure 4.21 Optimized Part E FEA results (a) von mises stress results for the optimized Part E (b) deflection results for the optimized Part E

Figure 4.22 shows the FEA results for the optimized upper arm. As seen in this figure, the stresses generated upon the upper arm part may have exceeded the 20MPa yield stress level by a slight value of 0.368MPa but it does not exceed the new maximum yield stress of 21MPa. Moreover the deflection of this part is also lower than 5mm. Thus this part is considered to be functional.

The reason for the stresses to exceed the 20MPa mark may be due to the upper arm part's own weight that is not taken into consideration during calculation that could have resulted in the forces acting on this part to be larger than calculated.

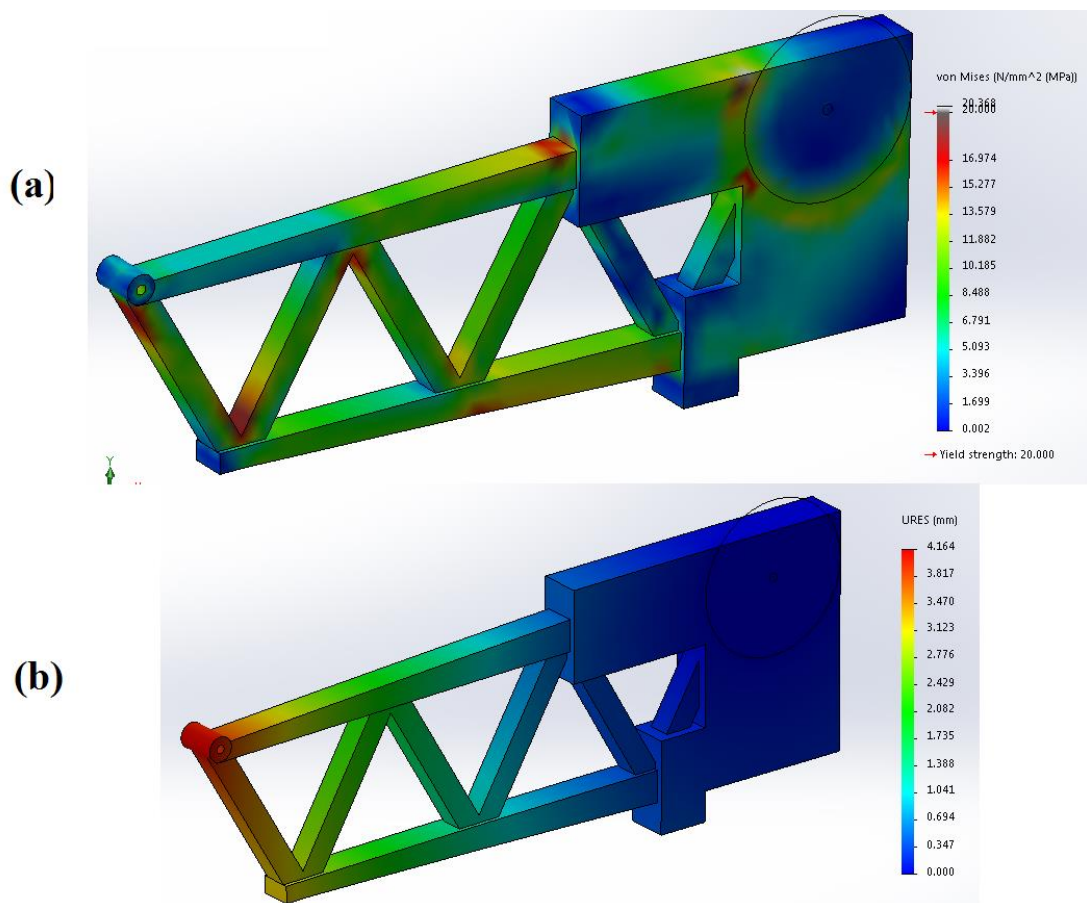


Figure 4.22 Optimized Upper Arm FEA results(a) von mises stress results for the optimized upper arm (b) deflection results for the optimized upper arm

Figure 4.23 shows the FEA results of the optimized part B. As seen in this figure, the stresses generated upon the optimized part B is below the 21MPa range and its deflection is also below the 5mm. Thus the part is deemed functional. Comparing the deflection results for both the un-optimized and optimized part B shown in Figure 4.15 (b) and Figure 4.23 (b) respectively, the optimized part B has a lower deflection.

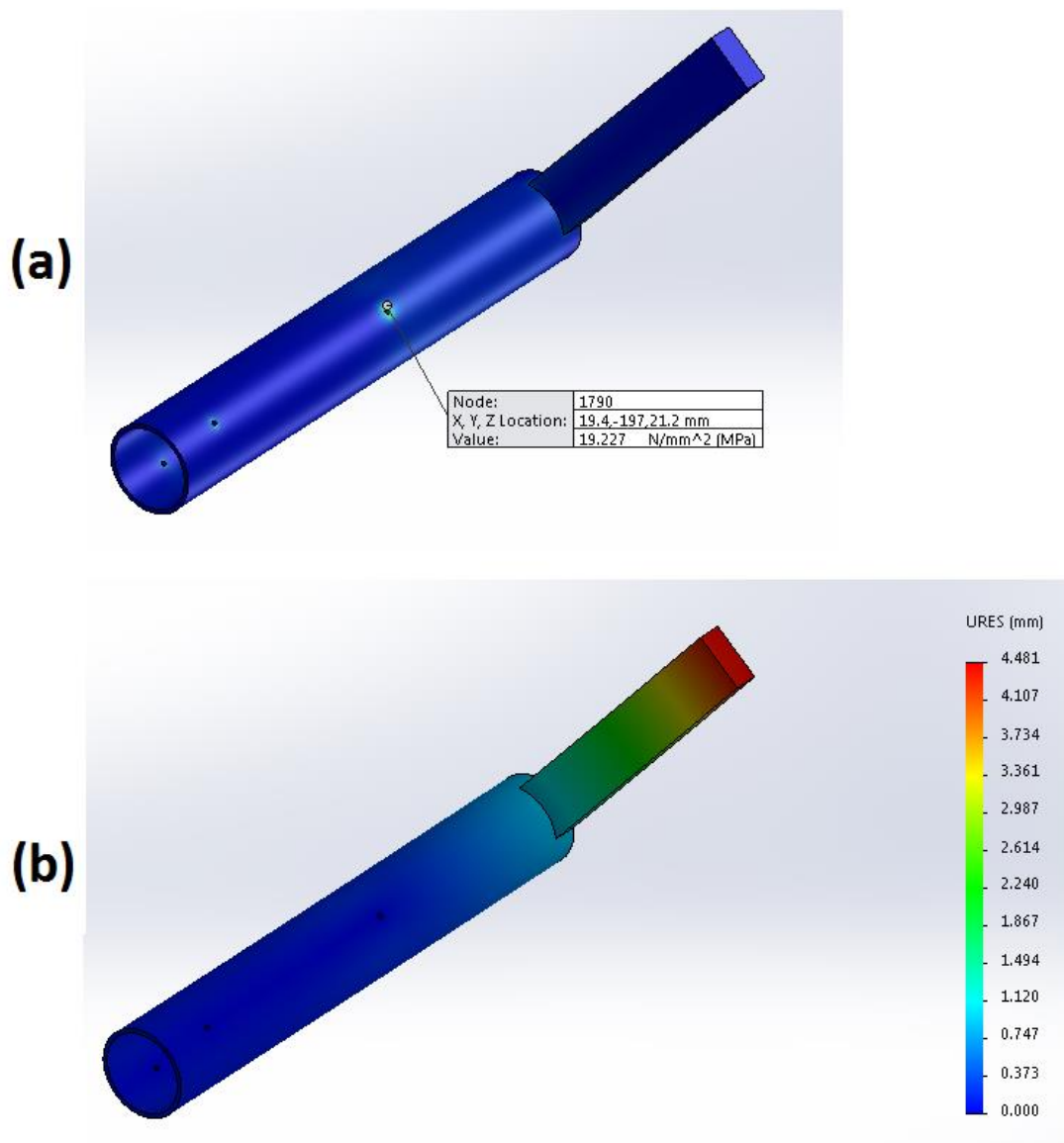


Figure 4.23 Optimized part B FEA results(a) von mises stress results for the optimized Part B (b) deflection results for the optimized Part B

Figure 4.24 shows the FEA results for the optimized lower arm part. As seen in this figure, the stresses generated upon the optimized lower arm part are below the 21MPa range and its deflection is also below the 5mm. Thus the part is deemed functional.

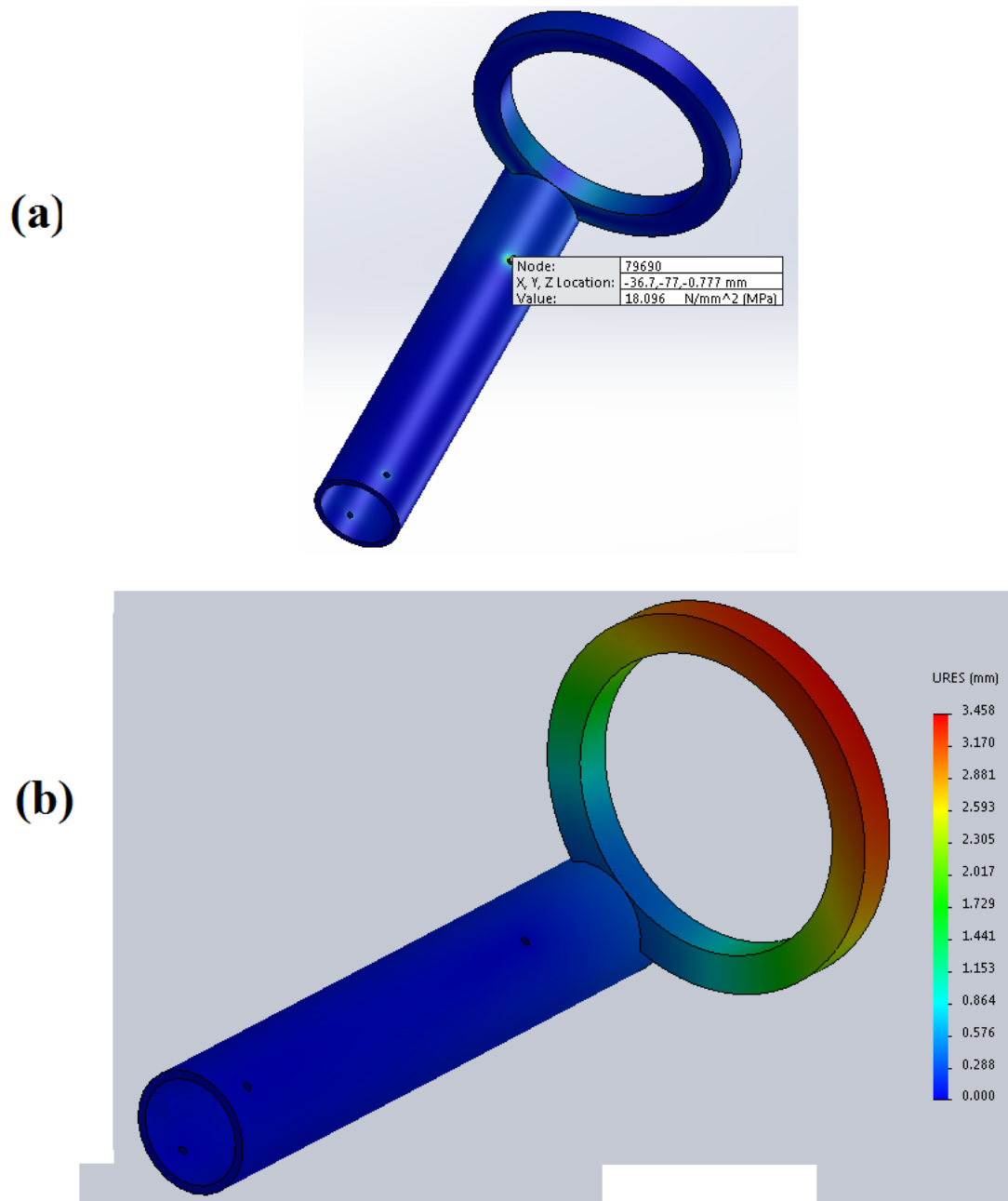


Figure 4.24 Optimized Lower Arm FEA results(a) von mises stress results for the optimized Lower arm (b)

Although the deflection for the optimized Part D, E and the upperarm were not calculated, the FEA results showed a striking difference where the deflections of all the optimized chosen parts are lower than the un-optimized parts.

The weight of the optimized parts is lower than their un-optimized counterparts. This may have resulted in lesser loads acting upon the optimized parts leading to lesser deflections when compared to their un-optimized counterparts.

Thus the FEA results suggest that the stresses and deflections generated upon the optimized parts are within the limits of the maximum allowable yield stress and deflections unlike their un-optimized counterparts.

4.10 Discussion

Table 2 shows the mass for the parts that were modelled and simulated in Solidworks. The masses for both the optimized and un-optimized parts shown in Table 2 were obtain by selecting the 'mass properties' function from the 'Evaluate' tab available in Solidworks (Saari, 2011).

Table 2 Mass of the parts

	Un-optimized Exoskeleton Parts	optimized Exoskeleton Parts
Part E	350.67 grams	178.61 grams
Part D	288.27 grams	115.87 grams
Upperarm	774.23 grams	475.40 grams
Lowerarm	569.43 grams	509.04 grams
Part B	1033.24 grams	771.04 grams

The FEA simulation results has been generated for the optimized and un-optimized, 3D modelled parts of the exoskeleton.

The proposed exoskeleton has been sketched and its parts have been chosen, calculated, modelled, undergo stress analysis and structural optimization to produce an optimized version of these parts. These optimized parts has also been calculated, modelled and undergo stress analysis. The FEA results suggest that the stresses generated upon the optimized parts are within the limits of the maximum allowable yield stress and deflections unlike their un-optimized counterparts.

The achievement obtained from this study is the development of an exoskeleton that is capable of transmitting the input torque mechanically from the base to the limbs without the use of cables, pneumatic and hydraulic pistons.

By performing, structural optimization onto the proposed exoskeleton's parallelogram linkage actuators, the weight of these actuators were reduce. This results in these actuators being able to apply more torque onto its limbs. Thus the power transmission system is considered to be optimized.

The reason for structurally optimizing the developed exoskeleton however is to reduce its weight as much as possible. The reduction of the exoskeleton weight reduces the material cost of the exoskeleton due to the weight of its limbs. This result in the increase of the maximum load capacity of the developed exoskeleton. Thus by structurally optimizing the developed exoskeleton, the exoskeleton is improved further to enhance its competitive edge in terms of cost reduction, weight reduction and maximum load carrying capabilities. However, this exoskeleton is not meant for high speed applications nor is it aesthetically appealing but rather it is focused on generating resistive forces onto the patients arm for medical purposes.

The wrist twisting motion of the proposed exoskeleton however needs an electric motor with a torque that doubles the 9.1Nm torque produced by the forearm's twisting motion. However, this value of 18.2Nm torque is considered small when compared to the required torque of 72.5Nm for the forearm and 125Nm for the upperarm. This gives an opportunity for other researchers to develop a new and improve system for part B's mechanical principal to reduce the required torque of the exoskeleton forearm's twisting motion of 18.2Nm.

Part A of the proposed exoskeleton version shown in Figure 4.1 was not chosen to be optimized in this report because it is viewed separately from the chosen mechanical actuators of parallelogram1 and parallelogram2 shown in this figure. Thus the structural optimization for part A is reserved for future research.

More upperarm parts can be implemented into the proposed exoskeleton design to increase its safety and structural integrity but such implementation is reserved for future research.

Actuators and electronic components can be pre-bought from the market, assembled and implemented into the developed exoskeleton for robotic control but this task is reserved for future research.

CHAPTER 5

CONCLUSION AND FUTURE WORKS

5.1 Conclusion

As shown in Table 2, the chosen parts of the exoskeleton has been optimized. Moreover, the research cycle shown in Figure 3.1 has been carried out. The FEA results of the optimized parts shows that the stresses and deflections generated are within the limits of the maximum allowable yield stress and deflections. The FEA results for some of the un-optimized parts however have exceeded the maximum allowable yield stress and deflections. This means the optimized parts of the exoskeleton are deemed functional while some of the un-optimized parts are deemed not functional. There is no need to recalculate and remodel the un-optimized parts as their optimized counter parts have already superseded them.

The achievement obtained from this study is the development of an exoskeleton that is capable of transmitting the input torque mechanically from the base to the limbs without the use of cables, pneumatic and hydraulic pistons. This achievement is also to the author's knowledge the novelty of this study. By reducing the weight of the parallelogram linkage actuators of the exoskeleton through the structural optimization processes, these actuators becomes lighter. This leads to the parallelogram linkage actuators being able to transmit more torque from the base to the limbs due to its weight reduction. Thus the power transmission system has been optimized.

There is a possibility that this exoskeleton can be used to improve the current existing exoskeletons in hospitals that have actuators positioned at their joints.

The exoskeleton has been developed and optimized and the research methodology has been carried out and completed. There is a possibility that this exoskeleton could be used to improve the existing exoskeletons in hospitals that have actuators positioned at their joints.

5.2 Future works

Part B's mechanical principal gives an opportunity for other researchers to develop a new and improve system to reduce the required torque of the exoskeleton forearm's twisting motion of 18.2Nm.

Part A of the proposed exoskeleton version shown in Figure 4.1 was not chosen to be optimized in this report because it is viewed separately from the mechanical actuators of parallelogram 1 and parallelogram 2 shown in this figure. Moreover, optimizing this part would require a lot of amendments in the calculations for some of the exoskeleton's parts. Thus the structural optimization of Part A is reserved for future research.

Actuators and electronic components can be purchased, assembled and programmed before it is implemented into the developed exoskeleton but this task is reserved for future research.

More upperarm parts can be implemented into the developed exoskeleton to increase its structural integrity and safety but such implementation is reserved for future research.

REFERENCES

- Abbey, T., 2016. *Finite Element Analysis Training: Basic Stiffness, Lesson 2*. [video online] Available at: <<https://www.youtube.com/watch?v=ZYcXJp6X5Tw>> [Accessed 15 November 2016].
- Abbey, T., 2016. *B3 - Finite Element Analysis Training: Basic Stiffness. Lesson 3*. [video online] Available at: <https://www.youtube.com/watch?v=C_SC4ZLx6zk> [Accessed 15 November 2016]
- Amy .S, 2012. *Gear Teeth Stresses on Polylactic and Steel Gears Friction and Wear of Materials Fall 2012*. [Online] Available at: <<http://www.ewp.rpi.edu/hartford/~sissaa/FWM/Project/GEAR%20TEETH%20STRESSES.pdf>> [Accessed 15 November 2016]
- Blender Foundation, 2016. *About - Blender.org – Home of the Blender Project – Free and Open 3D creation Software*. [Online] Available at: <<https://www.blender.org/about/>> [Accessed 7 July 2016]
- DassaultSystemes SolidWorks Corporation, 2016. *3D Cad Design Software Solidworks*. [Online] Available at: <<http://www.solidworks.com/>> [Accessed 7 July 2016]
- DassaultSystèmes, 1995-2016. *Material Properties Used in Solidworks Simulation*. [Online] Available at: <http://help.solidworks.com/2012/English/SolidWorks/cworks/ID_Available_Material_Properties.htm> [Accessed 15 November 2016]

- Farsetti, S., Cioni, B. and Lazzeri, A., 2011. Physico-Mechanical Properties of Biodegradable Rubber Toughened Polymers. *Macromolecular Symposia*. 301(1), pp. 82-89.
- Frisoli, A., Rocchi, F., Marcheschi, S., Dettori, A., Salsedo, F., Bergamasco, M., 2005. A new force-feedback arm exoskeleton for haptic interaction in Virtual Environments. In: *Proceedings of the First Joint Eurohaptics Conference and Symposium on Haptic Interfaces for Virtual Environment and Teleoperat or Systems*. Italy, 18-20 March 2005. Italy: IEEE.
- Gijbels, D., Lamers, I., Kerkhofs, L., Alders, G., Knippenberg, E., Feys, P., 2011. The Armeo Spring as training tool to improve upper limb functionality in multiple sclerosis: a pilot study. *Journal of neuroengineering and rehabilitation*. 8(1), pp. 5.
- Gopura, R. A. R. C., Kazuo K., Bandara, D. S. V., 2011. A brief review on upper extremity robotic exoskeleton systems. In: *2011 6th International Conference on Industrial and Information Systems, ICIIS 2011*. Sri Lanka, 16-19 Aug 2011, Kandy, Sri Lanka: IEEE.
- Juvinall, R. C., Marshek, K. M., 2000. *Fundamentals of Machine Component Design*. 3rd Ed. USA: John Wiley & Sons
- Kurowski, P., et Dvorak, P. ed, 2011. *Easily made errors mar FEA results* [Online] Available at :<<http://machinedesign.com/archive/easily-made-errors-mar-fea-results>> [Accessed 11 November 2016]
- Lovett, T., 2013. *Trusses, Method of Joints*. [Online] Available at: <<http://www.learneasy.info/MDME/MEMmods/MEM30005A/trusses/truss-example-working/truss-by-MoJ.html>> [Accessed 11 November 2016]
- MakeItFrom.com, 2016. *Polylactic Acid (PLA, Polylactide)*. [Online] Last updated on 016-08-06, Available at: <<http://www.makeitfrom.com/material-properties/Polylactic-Acid-PLA-Polylactide/#Intro>> [Accessed 15 November 2016]

- Myszka D. H., 2005. *Machines and Mechanisms : applied kinematics analysis*, 3rd ed. Upper Saddle River, NJ: Prentice Hall,
- Naidu, D., Stopforth, R., Bright, G., Shaniel, D., 2011. A 7 DOF exoskeleton arm: shoulder, elbow, wrist and hand mechanism for assistance to upper limb disabled individuals. In: *IEEEAFRICON 2011*, Zambia, 13 - 15 September 2011, Livingstone, Zambia: IEEE.
- Naidu, D., 2011, *Bio-Mechatronic Implementation of a Portable Upper Limb Rehabilitative Exoskeleton*. Masters. University of KwaZulu-Natal. Available at: <<http://citeseerx.ist.psu.edu/viewdoc/download?doi=10.1.1.828.2523&rep=rep1&type=pdf>> [Accessed 13 November 2016]
- Sanchez, R. J., Jr., Wolbrecht, E., Smith, R., Liu, J., Rao, S., Cramer, S., Rahman, T., Bobrow, J. E. and Reinkensmeyer, D. J., 2005. A pneumatic robot for re-training arm movement after stroke: Rationale and mechanical design. In: *9th International Conference on Rehabilitation Robotics*. Chicago, 28 June – 1 July 2005. Chicago: IEEE.
- Saari, R., 2011. Re: How to know the weight of a part?. *How to know the weight of a part?*. [blog] 14 November 2011. Available at: <<https://forum.solidworks.com/message/258450#49635>> [Accessed 13 December 2016]
- Shuvom G., 2015. *Choosing Your 3D Printing Material:It's About More Than Strength!*. [Online] Available at: <<http://blog.capinc.com/2015/01/choosing-your-3d-printing-material-its-about-more-than-strength/>> [Accessed 8 November 2016]
- Tigerquest.com, 2016. *Polar Moment of Inertia*. [Online] Available at: <<http://tigerquest.com/Mechanical/Strength%20of%20Materials/polar%20moment%20of%20inertia.php>> [Accessed 10 November 2016]

Learn Easy, 2013. *Combined Stresses*. [Online] Available at: <<http://www.learneasy.info/MDME/MEMmods/MEM09155A-CAE/070-Combined-Stresses/Combined-Stresses.html>> [Accessed 10 November 2016]

Pandhare A. P., Chaskar S. T., Patil J. N., Jagtap A. S., Bangal P. M., 2014, Design, Analysis And Optimization Of Skid Base Frame, *INTERNATIONAL JOURNAL OF TECHNOLOGY ENHANCEMENTS AND EMERGING ENGINEERING RESEARCH* [e-journal] 2(7), pp. 110-113. Available at: <<http://www.ijtee.org/final-print/july2014/Design-Analysis-And-Optimization-Of-Skid-Base-Frame.pdf>> [Accessed 29 Nov 2016].

Pytel, A., et Kiusalaas, J., 2012. *Mechanics of materials*, 2nd Ed. USA : Cengage Learning

Ugural, A. C., 2008. *Mechanics of materials*, USA : John Wiley & Sons.

Walter, F., 2013. *How to Identify and Resolve Singularities in the Model when Meshing* [Blog] 29 October 2013. Available at :<<https://www.comsol.com/blogs/how-identify-resolve-singularities-model-meshing/>> [Accessed 11 November 2016]

Wu, T. M., Wang, S. Y., Chen, D. Z., 2011. Design of an exoskeleton for strengthening the upper limb muscle for overextension injury prevention, *Mechanism and Machine Theory*. 46(12), pp. 1825-1839.

Zhao, Y., Zhang, W., Ge, W., & Li, S., 2013. Finite Element Simulation of Soldier Lower Extremity Exoskeleton, *Journal Of Multimedia*. 8(6), pp. 705-711.